CHALMERS
UNIVERSITY OF TECHNOLOGY

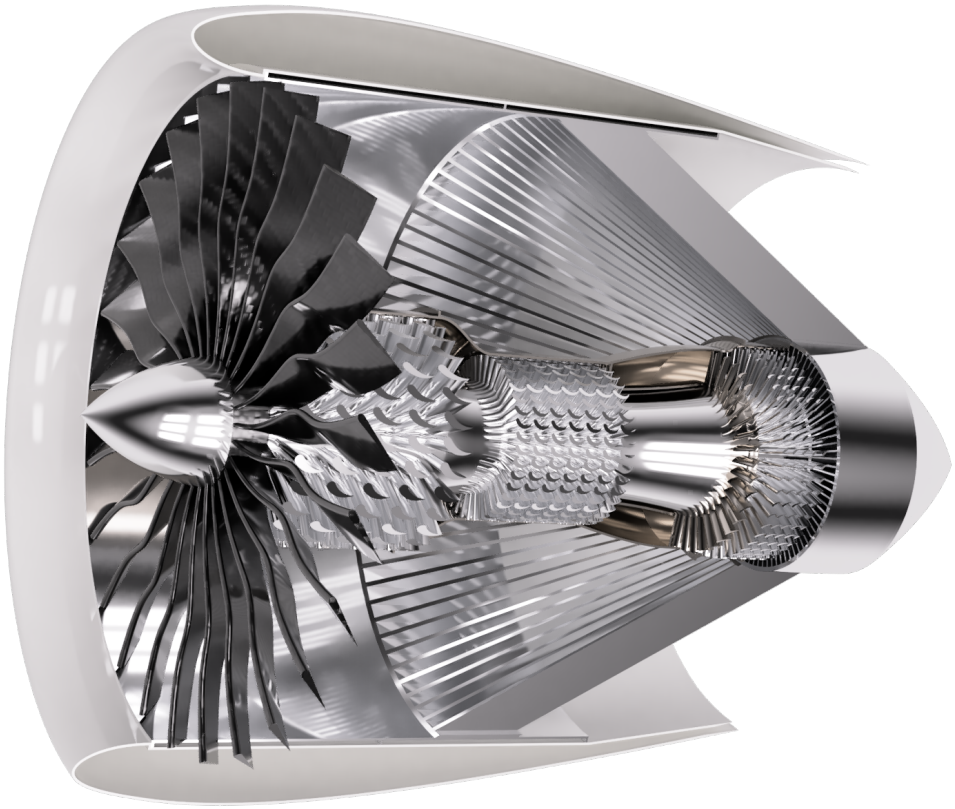

Modelling and simulation of the Water Enhanced Turbofan concept

Master's thesis in Mobility Engineering

FILIP HERBERTSSON

DEPARTMENT OF MECHANICS AND MARITIME SCIENCES

CHALMERS UNIVERSITY OF TECHNOLOGY
Gothenburg, Sweden 2024
www.chalmers.se

Master's thesis 2024

Modelling and simulation of the Water Enhanced Turbofan concept

FILIP HERBERTSSON

CHALMERS
UNIVERSITY OF TECHNOLOGY

Department of Mechanics and Maritime Sciences
Division of Fluid Dynamics
Turbomachinery & Aeroacoustics
Chalmers University of Technology
Gothenburg, Sweden 2024

Modelling and simulation of the Water Enhanced Turbofan concept
FILIP HERBERTSSON

Supervisor: Tomas Grönstedt, Department of Mechanics and Maritime Sciences
Examiner: Tomas Grönstedt, Department of Mechanics and Maritime Sciences

Master's Thesis 2024
Department of Mechanics and Maritime Sciences
Division of Fluid Dynamics
Turbomachinery & Aeroacoustics
Chalmers University of Technology
SE-412 96 Gothenburg
Telephone +46 31 772 1000

Cover: Visualization of a Water Enhanced Turbofan cycle engine.

Typeset in LaTeX
Printed by Chalmers Reproservice
Gothenburg, Sweden 2024

Modelling and simulation of the Water Enhanced Turbofan concept
FILIP HERBERTSSON
Department of Mechanics and Maritime Sciences
Chalmers University of Technology

Abstract

The aviation industry needs to reduce its climate impact. The Water Enhanced Turbofan (WET) is a new engine technology that could reduce the climate impact from aviation with regards to carbon dioxide (CO_2) emissions, nitrogen oxides (NO_x) emissions and contrail formation. In the WET cycle, water is injected into the combustion chamber, which lowers the formation of NO_x-gases. The water also increases the thermodynamic efficiency of the turbines, and is collected through a set of heat exchangers so that it can be pumped back into the combustion chamber. If more water is collected than what was injected, the exhaust stream will contain less water that has the potential to produce contrails.

In this work, a WET cycle engine and the components it consists from are modeled, based on a reference engine from previous Chalmers research and the most recent WET cycle concept from MTU Aero Engines. The concept engine is analysed through selected cycle design parameters, as well as through generalized geometric parameters (GGP) of the heat exchangers. The design point is optimized with respect to specific fuel consumption (SFC), and the benefits of the water injection are analysed.

It is estimated that, by careful selection of cycle parameters, CO_2-emissions can be reduced by more than 7% and NO_x-emissions can be reduced by more than 85%. This is in fair agreement with the benefits that MTU Aero Engines predicts. Limiting factors include the weights of the WET cycle components, the size of the engine as well as the temperature that the low pressure turbine (LPT) can handle. It is proposed that, in order to obtain further benefits, other cycle parameters should be analysed such as the overall pressure ratio (OPR) and the amount of cooling flow. Further, to remove the limit of LPT temperature, the LPT could be cooled by air from the compressor stages.

Keywords: Water Enhanced Turbofan, CO_2 emissions, NO_x emissions, cycle optimization, GESTPAN, modelling, simulation

Acknowledgements

I would like to thank my supervisor and examiner Tomas Grönstedt for his support and guidance throughout the project, and for believing in me and giving me this opportunity. I would also like to thank Xin Zhao for providing tables with humid gas properties. Also, a big thanks goes to Petter Miltén for providing the equations for heat exchanger property estimates, and for helping out during troubleshooting. Finally, I would like to thank my girlfriend Elin Johansson, for always being there for me throughout my studies.

Filip Herbertsson, Gothenburg, June 2024

List of Acronyms

Below is the list of acronyms that have been used throughout this thesis listed in alphabetical order:

BPR	Bypass Ratio
CO_2	Carbon Dioxide
FAR	Fuel-to-Air Ratio
GESTPAN	GEneral Stationary and Transient Propulsion ANalysis
GGP	Generalized Geometrical Parameter
HPC	High Pressure Compressor
HPT	High Pressure Turbine
HRSG	Heat Recovery Steam Generator
HX	Heat Exchanger
IAPWS	The International Association for the Properties of Water and Steam
IPC	Intermediate Pressure Compressor
LMTD	Logarithmic Mean Temperature Difference
LPT	Low Pressure Turbine
NO_x	Nitrogen Oxides
OPR	Overall Pressure Ratio
SFC	Specific Fuel Consumption
TOC	Top-Of-Climb
VIND	Virtuell Integrerad Demonstrator för turbomaskiner
WAR	Water-to-Air Ratio
WET	Water Enhanced Turbine
WRF	Water Recovery Factor

Nomenclature

Below is the nomenclature of indices, subscripts, superscripts, and variables that have been used throughout this thesis.

Indices

i,j	Indices for constants
f	Fluid index

Subscripts

cc	Combustion chamber
con	Condensed
π	Partial derivative with respect to π
τ	Partial derivative with respect to τ
ff	Free-flow
fin	Fin
fr	Frontal
$fuel$	Fuel
id	Ideal
in	Inlet
$loss$	Loss
m	Mean
NOx	Nitrogen oxides
o	Overall
out	Outlet
p	Propulsive
$pump$	Pump

R	Reference
s	Solid
sat	Saturation
t	Total
th	Thermal
w	Wetted
W	Wall

Superscripts

$\circ$	Ideal-gas part
r	Residual part
$*$	Reference
-	Normalized

Variables

Latin alphabet

A	Area
c_p	Isobaric specific heat capacity
c_V	Isochoric specific heat capacity
d	Characteristic length
EI	Emission index
f	Friction coefficient
g	Gravitational constant
h	Heat transfer coefficient
ΔH	Change in enthalpy
ΔH_{latent}	Change in enthalpy due to evaporation
j	j-factor
k	Thermal conductivity
ℓ	Undisturbed flow length
$\frac{l_f}{\sqrt{t_f}}$	Characteristic dimension
L	Length

m	Mass
$\dot{m}$	Mass flow rate
p	Static pressure
p_0	Stagnation pressure
P	Power
Pr	Prandtl number
$\dot{q}$	Heat flux
$\dot{Q}$	Heat per unit time
R	Gas constant
Re	Reynolds number
R_{STM}	Steam correction factor
t	Wall thickness
T	Temperature
ΔT_A	Temperature difference at end A
ΔT_B	Temperature difference at end B
ΔT_{ISA}	Temperature difference from the International Standard Atmosphere
ΔT_{lm}	Logarithmic mean temperature difference
TF	Technology factor
U	Overall heat transfer coefficient
v	Flow velocity
V_t	Volume
WAR	Water-to-air ratio
WRF	Water Revovery Factor
x	Site along component
Z	Altitude

Greek alphabet

α	Surface-area density
α_r	Surface-area-density ratio
η	Efficiency
κ_T	Isothermal compressibility
λ	Ratio of specific heats
μ	Dynamic viscosity

ν	Kinematic viscosity
π	Normalized pressure
ρ	Density
σ	Void fraction
σ_r	Void-fraction ratio
σ_{ftt}	Finned-to-total-surface-area ratio
τ	Normalized temperature
ϕ	Number of passes
χ	Solid volume fraction
Ψ	Pressure head

Functions and constants

F	Constants
G	Constants
I	Constants
J	Constants
K	Constants
ml	Function
n	Constants
$\bar{q}_D$	Constant
v	Constant
y	Function
Z	Function
β	Function
γ	Function
Γ_0	Constant
ζ	Function
ϑ	Function
Λ	Constant
ξ	Function
$\Delta\bar{\chi}$	Function

Contents

List of Figures

List of Tables

1
Introduction

1.1 Background

The aviation industry needs to reduce its climate impact, just like all other industries. However, unlike most other industries, the aviation industry requires high power and low weight propulsion systems that can run for hours without the need to refuel. In general, these propulsion systems impact the climate in three ways. Firstly, jet fuel is carbon based and thus produces carbon dioxide (CO_2) when combusted, which is a greenhouse gas that contributes to global warming [1]. This gives a high importance to increase fuel efficiency in order to reduce the total fuel consumption and thus the CO_2 emissions. Secondly, the high temperatures involved in combustion leads to formation of nitrogen oxides (NO_x) from the nitrogen present in the atmosphere. Aviation is responsible for a large portion of the anthropogenic emission of NO_x in the upper troposphere [2], and chemical reactions with the atmosphere lead to the production of ozone [3] amongst other. Lastly, water that is either present in the atmosphere or is produced by the combustion lead to the formation of contrails. Contrails also contribute to global warming as they increase the radiative forcing [1].

The Water Enhanced Turbofan (WET) is a new turbofan technology that could reduce the climate impact from aviation in all three areas [4]–[8]. In the WET cycle concept, water is injected into the combustion chamber [4]–[6]. After the turbine stages of the engine, the exhaust gases are cooled by water and by excess air which makes the water in the exhaust condense. The water that was recovered can then be used to cool more exhaust gas and be put back into the cycle. Overall, this system promises higher fuel efficiency, which helps to reduce the CO_2-emissions [4], [6]. The water also lowers combustion temperature and reduces the amount of NO_x-emissions [4], [6], [9]. However, some note that carbon monoxide (CO) emissions increase with water injection [7], and others have noted better performance if the water is injected earlier than the combustion chamber [8].

Currently, the publicly available research on the WET cycle is limited. More research is needed to evaluate the proposed benefits of the WET cycle and what limitations there are. This research in the initial stage is valuable to the Department of Mechanics and Maritime Sciences as they plan further research in the area. Thus, this paper serves as a starting point for future research or as a help in down-selection of research areas of importance within the WET cycle concept. Furthermore, the models and code developed in the project can be directly used in future research as well, as the code will be written using their in-house software.

1.2 Aim

The main goal of the project is to evaluate the system efficiency and the proposed benefits of the WET cycle, as well as to find limitations and future areas of research. As part of this, theoretical models of the new components will be developed and the in-house gas turbine engine simulation tool GESTPAN will be augmented with these components. A model of the full WET cycle system will also be formulated in GESTPAN. The individual components and the full system model should be made such that other researchers at the department can use them.

There is no societal impact of the WET cycle, nor are there any relevant ethical aspects to consider. However, it is important to consider the technology from an ecological perspective. The project should answer to what degree the proposed benefits of the WET cycle are valid, and how they affect the total environmental impact of the system. On this topic, the weight of the system is also important as increased weight of the aircraft leads to higher fuel consumption, which could diminish some of the possible benefits of the system.

1.3 Limitations

Only the components that are specific to the WET cycle are of interest in this work. Other components and stages might need to be sized differently or have different specifications than the baseline engine, as defined in the previous VIND project [10], but no new models will be developed for these components. Furthermore, the components that are specific to the WET cycle should only be modeled using simple correlations and well-known theory. More detailed models of the WET cycle components are left for future research. In addition, the work should focus on the usage of the model at the design point.

2
Theory

The WET cycle is a turbofan concept in which water is injected into the combustion chamber. The water increases the total mass flow in the core which is expected to have multiple benefits, such as lower fuel consumption and lower NO_x production [4]–[8]. Furthermore, water increases the specific heat capacity of the exhaust gas which is thermodynamically beneficial [4]. To be able to have water flow throughout a flight without having to bring a lot of water with the aircraft, the water needs to be reused. First, the exhaust stream is cooled down using heat exchangers after which the water condenses and is extracted from the flow.

This chapter describes a common turbofan cycle that will be used as a reference cycle. Based on the reference cycle, the WET cycle is defined and models for the components are presented, as well as modifications needed to already established turbofan components. In order to model the WET cycle components, further information is given about heat exchangers. Lastly, models to estimate thermodynamic properties of gases and fluids are presented, as well as models to estimate emissions.

2.1 Reference cycle

Parameter	**Value**
Altitude (m)	10668
Mach number	0.84
ΔT_{ISA} (K)	10
Inlet flow (kg/s)	625.6
Fuel flow (kg/s)	1.0703
Cooling flow (kg/s)	7.0963
OPR	74.004
SFC (mg/Ns)	15.006
BPR	13.693
Thrust (kN)	71.324
Turbine inlet temperature (K)	1903.8

Table 2.1: Main parameters of the reference cycle at Top-Of-Climb (TOC).

In order to evaluate the WET cycle concept, it is applied to a reference cycle and compared. An estimate of a future engine is used as the reference, since the development of the necessary components for a WET-engine will take time. The reference cycle is a high bypass ratio, two-shaft, geared turbofan developed as part of the

Component	Efficiency	Pressure ratio
Inlet	-	0.997
Fan	0.91576	1.44
IPC	0.88736	3.465
HPC	0.86897	16.594
Burner	0.999	0.97
HPT	0.9287	-
LPT	0.93185	-
Bypass nozzle	-	0.982
Core nozzle	-	0.985

Table 2.2: Design efficiency and pressure ratios for selected components.

VIND project [10]. It represents what the researchers believe to be a good approximation of a future engine for the year 2035, intended for narrow body aircraft. It consists of a fan and a booster compressor connected to a low pressure turbine, of which the rotational speed of the fan has been reduced through gears. It also has a high pressure compressor connected to a high pressure turbine. Important parameters for the reference cycle is found in Table 2.1. The efficiencies and pressure ratios used are presented in Table 2.2.

2.2 WET cycle

The corresponding WET cycle model adds three new components to the system; the HRSG, the condenser and the pump. It also requires modification of some of the available components in order to take into account the water that is present.

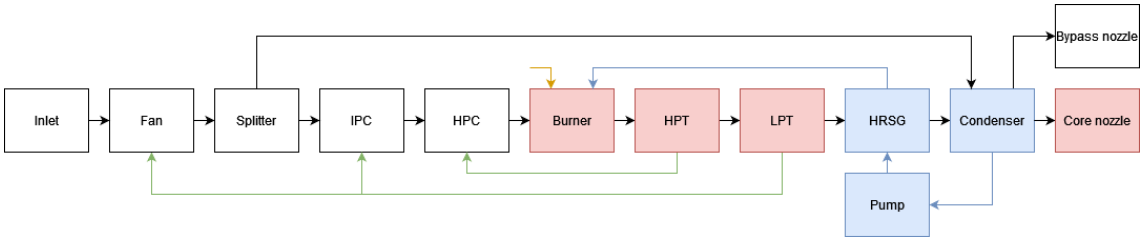

Figure 2.1: A diagram depicting the WET cycle components and their order with respect to the flow direction. Black arrows represent air or exhaust gas, blue arrows represent water, green arrows represent power and yellow arrows represent fuel. The white components were available in GESTPAN, the red components were available but needed modification, and the blue components are new and unique to the WET cycle.

A diagram of the investigated WET cycle is seen in Figure 2.1. In the WET cycle, water is injected into the combustion chamber. This increases the heat capacity of the core flow. After the exhaust air exits the last turbine, it enters the Heat Recovery Steam Generator (HRSG). The HRSG uses residual heat in the exhaust flow to evaporate and superheat the water before it is injected into the combustion

chamber. This brings some heat energy back to the combustion chamber and keeps it in the cycle loop [4]. The HRSG has the added benefit that it cools the exhaust flow which makes it easier in later steps to extract water from it. The HRSG is placed inside the core right after the last turbine stage, which constrains its size. For the most effective heat transfer, the HRSG is a counter-flow heat exchanger in which the two flows move in opposite directions [11].

After the exhaust exits the HRSG, it enters the condenser. The condenser is another counter-flow heat exchanger in which the exhaust is further cooled using air from the bypass channel [4]. The exhaust is cooled down enough so that it becomes supersaturated with water, and thus water condenses out of the exhaust. The condenser is placed in the bypass stream, such that exhaust gas travels from the back of the core to the front of the nacelle. The water recovery system, placed after the condenser in the nacelle, extracts the condensed water from the flow. The condensed water is collected through channels in the nacelle interior and is then pumped through the HRSG and into the combustion chamber.

The proposed advantages of using the WET cycle are many. As the recovered water is heated up and injected into the combustion chamber, heat from the exhaust is recovered and carried back into the thermodynamic cycle. At the same time, the temperature of the exhaust gas is reduced. Due to the injected water, the mass flow over the compressors is less than over the turbines. At the same time, water requires less energy to be pressurized than air. Furthermore, water injection increases the specific heat capacity of the exhaust gas, which makes it possible for the turbines to extract more energy. In total, this helps to increase the efficiency of the cycle which reduces fuel consumption and CO_2-emissions. The water will also decrease the temperature in the combustion chamber, and in turn decrease the amount of NO_x-emissions [9].

2.2.1 Heat Recovery Steam Generator

The Heat Recovery Steam Generator is the first step of the water recovery apparatus. It is a heat exchanger (HX) where exhaust gas enters through one channel and water enters through the other. The exhaust air from the turbines is cooled using water that has been recovered which makes it easier to extract water in the later stages of the exhaust. At the same time, the recovered water is evaporated and superheated, which brings heat back to the combustion chamber. The Logarithmic Mean Temperature Difference (LMTD) method [11] is used to calculate the heat fluxes throughout the heat exchanger. This procedure is described further in Section 2.3.1. However, extra care needs to be taken as this process involves both temperature change and phase change. In order to overcome this, the unit is split up into three sections: the economizer, the evaporator and the superheater [12]. A diagram of the HRSG that depicts the different sections is seen in Figure 2.2. In the economizer section, the liquid water is heated up to the boiling point. In the evaporator, the liquid water is evaporated into steam without a temperature increase. In the superheater, the steam is heated further. With this simplification, the fluid only experiences either a temperature change or a phase change at a single point in the component.

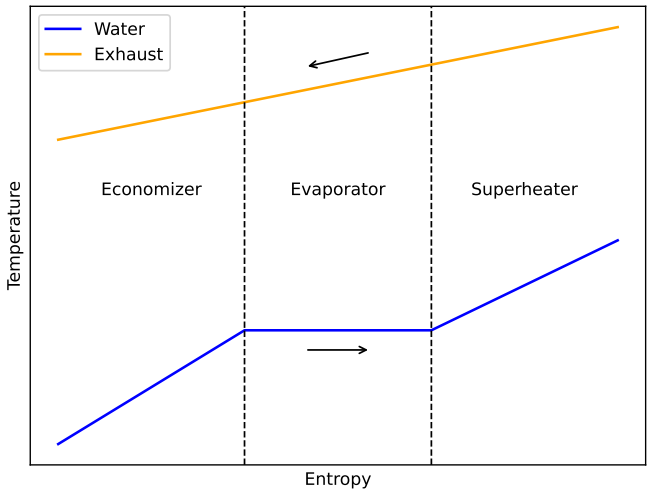

Figure 2.2: A diagram of the temperature changes that occurs in the exhaust gas and in the water inside the HRSG, divided into the three sections corresponding to the different processes. The arrows represent which direction the fluid flow occurs in.

The change in temperature of the cooling fluid with respect to the heat transferred is seen in Figure 2.2. For each of the theoretical sections, only temperature change or phase change occurs in each channel, which allows for the LMTD-method to be used. However, in reality, both temperature change and phase change occurs at the same time. This is especially true for the evaporator section. When there is a mixture of liquid water and steam, the liquid water will evaporate when heat is supplied, while the steam will increase in temperature. It is thus important to view this approach as an approximation.

2.2.2 Condenser and water recovery system

The condenser is the component responsible for recovering water from the exhaust stream and recycling it which makes it possible to keep the cycle running without an additional water supply. The air in the bypass channel is first used to cool the exhaust gas to the saturation point of water in an economizer section. Thereafter, the exhaust gas is further cooled while water is being condensed out of the flow in a condenser section. This section is difficult to model, as there is both a gas phase and a liquid phase. Furthermore, heat transferred away from the exhaust channel leads to both a temperature change and a phase change. It is not possible to split this section such that both temperature change and phase change do not occur in the same section, as was possible for the HRSG. Thus, the LMTD-method is less valid unless modified [11], [13]. The process that the water goes through is seen in Figure 2.3. In the economizer section, the temperature of the water decreases while the pressure remains virtually constant, except for pressure losses. This continues until the water reaches the saturation temperature at that pressure.

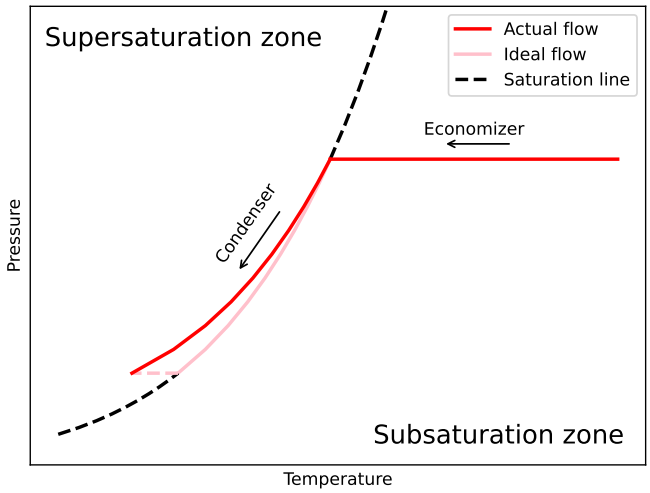

Figure 2.3: A temperature-pressure diagram of the water in the exhaust gas in the condenser. The pressure refers to the partial pressure of water. The dashed line represents the saturation pressure over liquid water.

After that, any further decrease in temperature leads to condensation of water, and a corresponding decrease in the partial pressure of the water in the exhaust which follows the saturation curve. In reality, as the condensation process happens quickly, some water does not have time to condense and the exhaust flow becomes supersaturated.

The bypass air experiences a pressure loss as it goes through the heat exchanger, which is negative in terms of thrust generation. Some of this loss in pressure is offset by the increase in temperature of the bypass air through the Meredith effect [4], as increased temperature means increased energy in the flow, which in turn generates thrust. A well designed heat exchanger allows for cooling of the exhaust flow with minimal loss of thrust.

The condensation process and water recovery is difficult to model at this stage of development. In order to properly evaluate how the water condenses and is recovered, a thorough study into the fluid-solid interaction in the condenser and nacelle is necessary. This requires a detailed design and is out of scope for this project. Instead, a simpler approach is taken. It is assumed that not all water that could condense will have time to condense and be collected by the recovery system. To model this, a Water Recovery Factor (WRF) is introduced. It is calculated as

$$WRF = \frac{\dot{m}_{con}}{\dot{m}_{con,id}}, \tag{2.1}$$

where $\dot{m}_{con}$ is the amount of water that is condensed and $\dot{m}_{con,id}$ is the amount of water that would be condensed given the current temperature, if the process was ideal. The water that is not condensed remains in the exhaust flow, and the exhaust thus becomes supersaturated.

2.2.3 Water pump

When the water is condensed, it needs be pumped to a higher pressure in order to be injected into the combustion chamber. This is done using a centrifugal pump. The minimum pressure the pump needs to achieve is the sum of the pressure in the combustion chamber and the pressure losses in piping and in the HRSG. The efficiency of the pump will not be 100%, which means that some losses will occur. It is assumed that theses losses will lead to a slight temperature increase in the fluid as well. With the assumption that both the inlet and the outlet conditions of the fluid are known, and that the water is incompressible, the pressure head at both ends are calculated by

$$\Psi = \frac{p}{\rho g} + \frac{v^2}{2g} + Z, \tag{2.2}$$

where g is the gravitational acceleration of the earth, ρ is the water density, v is the flow velocity and Z is the altitude of the water from a reference point [14]. The change in velocity and altitude is assumed to be negligible. Only the change in pressure head is of interest, thus the velocity and altitude terms are neglected. The change in pressure head $\Delta\Psi$ is related to the required power P by

$$P = \frac{g\Delta\Psi\dot{m}}{\eta_{pump}}, \tag{2.3}$$

where η_{pump} is the efficiency of the pump [14]. The losses, which will be converted to heat in the flow, is

$$P_{loss} = \dot{Q} = P(1 - \eta_{pump}). \tag{2.4}$$

Much less energy is used to increase the pressure of liquid water than is used to compress a gas. The magnitude of the water pump power requirement is thus much smaller than the powers involved in the turbines and compressors. In order to simplify the system, the power to drive the water pump is assumed to come from an external energy source and not from one of the shafts.

2.3 Heat exchangers

Heat exchangers (HX) are units that transfer heat from one fluid to another. They come in different shapes, such as tube-and-fin HX or plate HX. They are also divided based on the direction that the fluids flow in relation to one another, such as parallel flow, counter-flow and cross-flow. Both the HRSG and the condenser are, at their core, heat exchangers.

2.3.1 Heat transfer

In order for the heat exchangers to transfer heat, a temperature difference between the two fluids is needed. The larger the temperature difference, the more heat is transferred. However, the heat transfer also depends on material properties of the

fluids and the wall material. Instead of using heat transfer $\dot{Q}$, which is the amount of energy transferred per unit time, it is common to use heat flux $\dot{q}$, which is heat transfer divided by the area over which the heat is transferred.

Heat transfer is divided into three types; conduction, convection and radiation [11]. Conduction is heat transfer that happens within a material, for example from one side of a wall to the other. For conduction, the heat flux is written as

$$\dot{q} = -k\frac{\partial T}{\partial x}, \tag{2.5}$$

where k is the thermal conductivity and $\frac{\partial T}{\partial x}$ is the partial derivative of temperature across the material. Conduction happens in both fluids and solids. Convection on the other hand is the conductive heat transport due to movements in the flow, and is thus unique to heat transfers that involves fluids. For heat exchangers, convection occurs due to the interaction of the fluid with the solid structure. Convection depends on both material properties of the structure and properties of the flow. The convective heat transfer from a wall to a fluid (or vice versa) is

$$\dot{q} = h\left(T_W - T_f\right), \tag{2.6}$$

where h is the heat transfer coefficient, T_W is the wall temperature and T_f is the bulk fluid temperature. The heat transfer coefficient depends on flow properties, which is described with non-dimensional numbers. Two commonly used non-dimensional numbers are the Reynolds number and the Prandtl number. The Reynolds number is written as

$$\mathrm{Re} = \frac{vd}{\nu}, \tag{2.7}$$

where v is the bulk fluid velocity, d is a characteristic length of the system and ν is the kinematic viscosity. The Prandtl number is written as

$$\mathrm{Pr} = \frac{c_p\mu}{k}, \tag{2.8}$$

where c_p is the isobaric specific heat capacity and μ is the dynamic viscosity.

The last type of heat transfer is radiation. All bodies emit radiation that varies in intensity and wavelength with temperature. This radiation leads to a transfer of heat energy between bodies. For this analysis, the effect of radiation is neglected and focus is instead put on conduction and convection.

When heat is transferred to or from a fluid, it either experiences a temperature change, a phase change or both. The change in enthalpy ΔH that the fluid experiences is proportional to the heat transfer. Assuming constant specific heat throughout the temperature change, the sensible heat transfer is calculated as

$$\dot{Q} = \dot{m} \cdot \Delta H = \dot{m} \cdot c_p \cdot (T_{in} - T_{out}), \tag{2.9}$$

where $\dot{m}$ is the fluid mass flow, T_{in} is the inlet temperature and T_{out} is the outlet temperature. If instead the fluid experiences a phase change, the latent heat transfer is calculated as

$$\dot{Q} = \dot{m} \cdot \Delta H_{latent}, \tag{2.10}$$

where ΔH_{latent} is the enthalpy change due to phase change per unit mass.

To get the total heat flux across a heat exchanger it is possible to use the Logarithmic Mean Temperaure Difference (LMTD) method. For this, the logarithmic mean temperature difference ΔT_{lm} is needed, which is obtained as

$$\Delta T_{lm} = \frac{\Delta T_A - \Delta T_B}{\ln \Delta T_A - \ln \Delta T_B}, \tag{2.11}$$

where ΔT_A and ΔT_B are the differences in temperature between the fluids at end A and B respectively. If it is a parallel flow HX, end A contains both fluid inlets and end B contains both fluid outlets. If it is a counter-flow HX, end A contains the inlet of one fluid and the outlet of the other, and vice versa for end B. The heat transfer can then be obtained as

$$\dot{Q} = U \cdot A_w \cdot \Delta T_{lm}, \tag{2.12}$$

where U is the overall heat transfer coefficient for one side of the heat exchanger, and A_w is the wetted area of that side. U is a function of the heat transfer coefficients for the individual heat transfer processes that occurs in the heat exchanger, such as friction-induced convection in the fluids and conduction through the wall. The LMTD-method is valid when no phase change happens. However, it is possible to use the LMTD-method when one of the fluids experiences a phase change, given that the fluid that experiences a phase changes does not also experience a temperature change. In this case, the latent heat transfer is used instead of the sensible heat transfer.

2.3.2 Parameter estimation

It is difficult to evaluate heat exchangers and their performance. It requires deep knowledge about parameters of the flow as well as intricate knowledge about the geometry of the heat exchanger. To add to the complexity, different types of heat exchangers generally require different equations to describe them. In an attempt to simplify the estimation of heat exchanger properties for concept studies, a method was developed at Chalmers that only requires a few geometrical parameters as well as a few non-dimensional parameters [15]. This methodology can describe any heat exchanger and estimate the heat coefficient, the pressure loss as well as the weight of the system.

To begin with, it is necessary to specify the volume V_t, as well as the frontal area A_{fr}, of the heat exchanger. The frontal area is the area perpendicular to the direction of flow. The two channels do not need to have the same frontal area, however, since both HX are counter-flow, it is possible to treat the frontal areas as the same. From the volume and frontal area, the length L of the heat exchanger is found as

$$L = \frac{V_t}{A_{fr}}. \tag{2.13}$$

The length that the fluids flow might be longer than this and depends on the number of passes that the channels have. So, for each of the fluids f, the path length L_f is calculated as

$$L_f = L \cdot \phi_f, \tag{2.14}$$

where ϕ_f is the number of passes for fluid f. For each fluid (or channel), two parameters are defined. The first one is the surface-area density α, which is defined as

$$\alpha_f = \frac{A_{w,f}}{V_t}, \tag{2.15}$$

where $A_{w,f}$ is the wetted area of the channel for fluid f. The second parameter is the void fraction σ, which is defined as

$$\sigma_f = \frac{A_{ff,f}}{A_{fr}}, \tag{2.16}$$

where $A_{ff,f}$ is the free-flow area of the channel for fluid f. From these, two non-dimensional parameters are gotten. One is the surface-area-density ratio,

$$\alpha_r = \frac{\alpha_1}{\alpha_2}, \tag{2.17}$$

and the other is the void-fraction ratio

$$\sigma_r = \frac{\sigma_1}{\sigma_2}. \tag{2.18}$$

A third non-dimensional parameter, the solid volume fraction χ, is defined as

$$\chi = \frac{V_s}{V_t}, \tag{2.19}$$

where V_s is the volume of solid material in the heat exchanger. With α_r, σ_r and χ known, α_1, α_2, σ_1 and σ_2 are calculated through

$$\alpha_1 = \alpha_r \cdot \alpha_2 \tag{2.20}$$

$$\alpha_2 = \frac{2\chi}{t(\alpha_r + 1)} \tag{2.21}$$

$$\sigma_1 = \sigma_r \cdot \sigma_2 \tag{2.22}$$

$$\sigma_2 = \frac{1 - \chi}{1 + \sigma_r}, \tag{2.23}$$

where t is the thickness of the solid material in the internal channels of the heat exchanger. The solid volume fraction is also correlated to the weight m_s of the heat exchanger, through

$$m_s = \chi \cdot V_t \cdot \rho_s, \tag{2.24}$$

where ρ_s is the density of the solid material. The solid material is assumed to be aluminium with a density of $\rho_s = 2699\,\mathrm{kg/m^3}$. The weight represents the internal

weight of the heat exchanger, but excludes the weight of additional piping as well as structural components. For simplicity, it is estimated that these components add an additional 10% to the weight.

With the previously defined non-dimensional parameters, and a couple of geometric parameters, it is possible to estimate the heat transfer coefficient and the pressure loss of each side of the heat exchanger separately. The heat transfer coefficient h_f for channel f is found using the j-factor, j_f, according to Chilton-Colburn J-factor analogy, which relates heat, momentum and mass transfer. It states that

$$j_f = \frac{h_f}{c_{p,f} \cdot \dot{m}_f} \mathrm{Pr}_i^{\frac{2}{3}}. \tag{2.25}$$

The Prandtl number is calculated according to (2.8). The j-factor is estimated using

$$j_f = 0.360 \left(\frac{\ell \alpha_f}{4\sigma_f} \right)^{-0.401} \mathrm{Re}_f^{-0.413} + 2.13 \cdot 10^{-5} \left(\frac{\ell \alpha_f}{4\sigma_i} \right) \tag{2.26}$$

where ℓ is the undisturbed flow length and Re_f is the Reynolds number. This equation is an empirical relation obtained using data from heat exchangers for a wide variety of applications, some of which were developed over 60 years ago [15]. Better heat transfer is expected from modern day heat exchangers, especially given the stringent requirements of the aerospace industry. Thus, the j-factor is assumed to be 10% larger than the predictions. The Reynolds number of the flow is calculated by

$$\mathrm{Re}_f = \frac{4\dot{m}_f}{\alpha_f \mu_f A_{fr}}, \tag{2.27}$$

where $\dot{m}_f$ is the mass flow of fluid f and μ_f is the dynamic viscosity.

With the heat transfer coefficients for each channel, it is possible to get the overall heat transfer coefficient U_f. Since U_f relates the area of a channel and the temperature difference at the two ports of the heat exchanger with the heat that is transferred, it is different for each channel. For fluid 1, the overall heat transfer coefficient is expressed as

$$\frac{1}{U_1} = \frac{1}{(\eta_o h)_1} + \frac{2t}{\left(1 + \frac{1}{\alpha_r}\right) k_s} + \frac{\alpha_r}{(\eta_o h)_2}, \tag{2.28}$$

where t is the wall thickness, k_s is the thermal conductivity of the heat exchanger solid material and η_o is the overall surface efficiency. For aluminium, the thermal conductivity is $k_s = 237\,\mathrm{W/m\,K}$. When a channel does not have any fins, the overall surface efficiency becomes $\eta_o = 1$. If a channel has fins, the efficiency is expressed as

$$\eta_{o,f} = 1 - \sigma_{ftt,f}(1 - \eta_{fin}), \tag{2.29}$$

where $\sigma_{ftt,i}$ is the finned-to-total-surface-area ratio, and η_{fin} is the fin efficiency. If only one of the channels has fins, $\sigma_{ftt,f}$ is estimated by

$$\sigma_{ftt,2} = \frac{\alpha_2 - \alpha_1}{\alpha_2}. \tag{2.30}$$

In the case above, the channel for fluid 1 does not have fins but the channel for fluid 2 does. The fin efficiency in turn is estimated using

$$\eta_{fin} = \tanh(ml_{fin})/ml_{fin}, \tag{2.31}$$

where

$$ml_{fin} = \frac{l_{fin}}{\sqrt{t_{fin}}}\sqrt{\frac{2h_{fin}}{k_s}}, \tag{2.32}$$

where $\frac{l_{fin}}{\sqrt{t_{fin}}}$ is the characteristic dimension of the fins and h_{fin} is the heat transfer coefficient of the fins. It is difficult to estimate the properties of the fins, thus some simplifications are made. It is assumed that only one of the channels has fins. This assumption works well when one of the fluids is a liquid and the other is a gas [15], however, it works less well when both fluids are gases. The heat transfer coefficient of the fins is also assumed to be the same as the heat transfer coefficient of the channel that contains the fins.

The pressure loss in a channel, Δp_i, is related to the friction coefficient, f_i, according to

$$\Delta p_f = \frac{\dot{m}_f^2}{p_{0,in,f}A_{fr}^2}\left(\left(\frac{1}{\sigma_f^2}+1\right)\left(\frac{1}{\rho_{out,f}}-1\right)+\frac{f_f\alpha_f L_f}{\sigma_f^3\rho_{m,f}}\right) \tag{2.33}$$

where $p_{0,in,f}$ is the total pressure at the inlet, $\rho_{out,f}$ is the density at the exit, $\rho_{m,f}$ is the mean density and L_f is the length of the channel. Similarly to the j-factor, the friction coefficient is estimated using

$$f_f = 0.492\left(\frac{\ell\alpha_f}{4\sigma_f}\right)^{-0.501}\mathrm{Re}_f^{-0.232} \tag{2.34}$$

which has been obtained using data on previous heat exchangers. Better performance is expected from modern day heat exchangers which have been designed carefully, thus the pressure losses are reduced by 10% from this estimation.

2.4 Physical properties

Calculation of heat transfer coefficients requires good estimates of multiple thermodynamic properties of the fluids. Equations provided by The International Association for the Properties of Water and Steam (IAPWS) are used to make such estimates. With their nomenclature, water is divided up into five regions in a temperature-pressure-diagram, and each region has different equations that describe the thermodynamic properties [16]. In this work, region 1 and region 2 are of interest, as these represent liquid water and steam respectively and are within reasonable temperature and pressure limits for a turbofan engine. The industrial formulations were used, as these are easier to formulate and quicker to evaluate than the scientific equations, while they provide high accuracy.

2.4.1 Liquid water

With the temperature and the pressure of liquid water known, the thermodynamic properties are estimated using the function $\gamma(\pi, \tau)$, where pressure and temperature has been normalized such that $\pi = p/p^*$ and $\tau = T^*/T$ using constants p^* and T^*. The function is defined by

$$\gamma(\pi, \tau) = \sum_{i=1}^{34} n_i (7.1 - \pi)^{I_i} (\tau - 1.222)^{J_i}, \tag{2.35}$$

where n_i, I_i and J_i are constants provided by IAPWS (see Appendix A) [16]. Using the derivatives of this function the thermodynamic properties are found. Short-hand notation for the derivatives are

$$\gamma_\pi = \frac{\partial \gamma}{\partial \pi}(\pi, \tau) = -\sum_{i=1}^{34} n_i I_i (7.1 - \pi)^{I_i - 1} (\tau - 1.222)^{J_i} \tag{2.36}$$

$$\gamma_\tau = \frac{\partial \gamma}{\partial \tau}(\pi, \tau) = \sum_{i=1}^{34} n_i J_i (7.1 - \pi)^{I_i} (\tau - 1.222)^{J_i - 1} \tag{2.37}$$

$$\gamma_{\pi\pi} = \frac{\partial^2 \gamma}{\partial \pi^2}(\pi, \tau) = \sum_{i=1}^{34} n_i I_i (I_i - 1)(7.1 - \pi)^{I_i - 2} (\tau - 1.222)^{J_i} \tag{2.38}$$

$$\gamma_{\pi\tau} = \frac{\partial^2 \gamma}{\partial \pi \partial \tau}(\pi, \tau) = -\sum_{i=1}^{34} n_i I_i J_i (7.1 - \pi)^{I_i - 1} (\tau - 1.222)^{J_i - 1} \tag{2.39}$$

$$\gamma_{\tau\tau} = \frac{\partial^2 \gamma}{\partial \tau^2}(\pi, \tau) = \sum_{i=1}^{34} n_i J_i (J_i - 1)(7.1 - \pi)^{I_i} (\tau - 1.222)^{J_i - 2}. \tag{2.40}$$

With these derivatives, the density ρ is

$$\rho = \frac{p}{RT\pi\gamma_\pi}, \tag{2.41}$$

where R is the gas constant. The isobaric specific heat capacity c_p is

$$c_p = -R\tau^2 \gamma_{\tau\tau}, \tag{2.42}$$

and the isochoric specific heat capacity c_V is

$$c_V = -R\tau^2 \gamma_{\tau\tau} + R\frac{(\gamma_\pi - \tau\gamma_{\pi\tau})^2}{\gamma_{\pi\pi}}. \tag{2.43}$$

Furthermore, the isothermal compressibility κ_T is [17]

$$\kappa_T = -\frac{\pi\gamma_{\pi\pi}}{p\gamma_\pi}, \tag{2.44}$$

and the specific enthalpy is

$$h = RT\tau\gamma_\tau. \tag{2.45}$$

2.4.2 Steam

Similar to liquid water, the thermodynamic properties of steam are estimated using the function $\gamma(\pi, \tau)$, where pressure and temperature is normalized such that $\pi = p/p^*$ and $\tau = T^*/T$ using constants p^* and T^*. In this case, the function is defined by [16]

$$\gamma(\pi, \tau) = \gamma^\circ(\pi, \tau) + \gamma^r(\pi, \tau), \tag{2.46}$$

where $\gamma^\circ(\pi, \tau)$ and $\gamma^r(\pi, \tau)$ are the ideal-gas part and residual part respectively. The ideal-gas part is defined as

$$\gamma^\circ(\pi, \tau) = \ln \pi + \sum_{i=1}^{9} n_i^\circ \tau^{J_i^\circ}, \tag{2.47}$$

for constants n_i° and J_i°. The derivatives are

$$\gamma_\pi^\circ = \frac{\partial \gamma^\circ}{\partial \pi}(\pi, \tau) = \frac{1}{\pi} \tag{2.48}$$

$$\gamma_\tau^\circ = \frac{\partial \gamma^\circ}{\partial \tau}(\pi, \tau) = \sum_{i=1}^{9} n_i^\circ J_i^\circ \tau^{J_i^\circ - 1} \tag{2.49}$$

$$\gamma_{\tau\tau}^\circ = \frac{\partial^2 \gamma^\circ}{\partial \tau^2}(\pi, \tau) = \sum_{i=1}^{9} n_i^\circ J_i^\circ (J_i^\circ - 1)\tau^{J_i^\circ - 2}. \tag{2.50}$$

The residual part is defined as

$$\gamma^r(\pi, \tau) = \sum_{i=1}^{43} n_i \pi^{I_i} (\tau - 0.5)^{J_i}, \tag{2.51}$$

for constants n_i, I_i and J_i. The derivatives are

$$\gamma_\pi^r = \frac{\partial \gamma^r}{\partial \pi}(\pi, \tau) = \sum_{i=1}^{43} n_i I_i \pi^{I_i - 1} (\tau - 0.5)^{J_i} \tag{2.52}$$

$$\gamma_\tau^r = \frac{\partial \gamma^r}{\partial \tau}(\pi, \tau) = \sum_{i=1}^{43} n_i J_i \pi^{I_i} (\tau - 0.5)^{J_i - 1} \tag{2.53}$$

$$\gamma_{\pi\pi}^r = \frac{\partial^2 \gamma^r}{\partial \pi^2}(\pi, \tau) = \sum_{i=1}^{43} n_i I_i (I_i - 1) \pi^{I_i - 2} (\tau - 0.5)^{J_i} \tag{2.54}$$

$$\gamma_{\pi\tau}^r = \frac{\partial^2 \gamma^r}{\partial \pi \partial \tau}(\pi, \tau) = \sum_{i=1}^{43} n_i I_i J_i \pi^{I_i - 1} (\tau - 0.5)^{J_i - 1} \tag{2.55}$$

$$\gamma_{\tau\tau}^r = \frac{\partial^2 \gamma^r}{\partial \tau^2}(\pi, \tau) = \sum_{i=1}^{43} n_i J_i (J_i - 1) \pi^{I_i} (\tau - 0.5)^{J_i - 2}. \tag{2.56}$$

The thermodynamic properties are estimated using these derivatives. The density ρ is

$$\rho = \frac{p}{RT\pi \left(\gamma_\pi^\circ + \gamma_\pi^r\right)}. \tag{2.57}$$

The isobaric specific heat capacity c_p is

$$c_p = -R\tau^2 \left(\gamma^\circ_{\tau\tau} + \gamma^r_{\tau\tau}\right), \tag{2.58}$$

and the isochoric specific heat capacity c_V is

$$c_V = -R\tau^2 \left(\gamma^\circ_{\tau\tau} + \gamma^r_{\tau\tau}\right) - \frac{\left(1 + \pi\gamma^r_\pi - \pi\tau\gamma^r_{\pi\tau}\right)^2}{1 - \pi^2\gamma^r_{\pi\pi}}. \tag{2.59}$$

Furthermore, the isothermal compressibility κ_T is [17]

$$\kappa_T = \frac{1 - \pi^2\gamma^r_{\pi\pi}}{p\left(1 + \pi\gamma^r_\pi\right)}, \tag{2.60}$$

and the specific enthalpy is

$$h = RT\tau \left(\gamma^\circ_\tau + \gamma^r_\tau\right). \tag{2.61}$$

2.4.3 Common properties for both phases of water

Some thermodynamic properties of water do not depend on the phase of the water, but rather on the thermodynamic properties alone. One of these is the kinematic viscosity μ, which is estimated solely using the temperature and density of the water [18]. The normalized viscosity $\bar{\mu} = \mu/\mu^*$, where μ^* is a constant, is estimated using three terms as

$$\bar{\mu} = \bar{\mu}_0(\bar{T}) \cdot \bar{\mu}_1(\bar{T}, \bar{\rho}) \cdot \bar{\mu}_2(\bar{T}, \bar{\rho}), \tag{2.62}$$

where $\bar{T} = T/T^*$, $\bar{\rho} = \rho/\rho^*$, and T^*, ρ^* are constants. The first factor $\bar{\mu}_0$ is

$$\bar{\mu}_0(\bar{T}, \bar{\rho}) = \frac{100\sqrt{\bar{T}}}{\sum_{i=0}^{3} \frac{F_i}{\bar{T}^i}}, \tag{2.63}$$

where F_i are constants. The second factor $\bar{\mu}_1$ is

$$\bar{\mu}_1(\bar{T}, \bar{\rho}) = \exp\left(\bar{\rho} \sum_{i=0}^{5} \left(\frac{1}{\bar{T}} - 1\right)^i \sum_{j=0}^{6} G_{ij}(\bar{\rho} - 1)^j\right). \tag{2.64}$$

where G_{ij} are constants. The third factor, called the "critical enhancement", takes into account effects that are seen close to the critical point of water. Because the critical point is well outside the pressure levels expected in the water system, this factor is simplified to $\bar{\mu}_2(\bar{T}, \bar{\rho}) = 1$. The total error in the viscosity estimate is up to 3% and it is slightly lower at lower temperatures than at higher temperatures.

Another property which is estimated similarly in both liquid water and steam is the thermal conductivity k. It depends on the temperature and density, but also requires the isobaric and isochoric specific heat capacities, the isothermal compressibility as well as the kinematic viscosity [19]. The normalized thermal conductivity $\bar{k} = k/k^*$, where k^* is a constant, is estimated using three parts through

$$\bar{k} = \bar{k}_0(\bar{T}) \cdot \bar{k}_1(\bar{T}, \bar{\rho}) + \bar{k}_2(\bar{T}, \bar{\rho}, \bar{c_p}, \lambda, \bar{\mu}), \tag{2.65}$$

where $\bar{c_p} = c_p/R$, R is the gas constant, $\lambda = c_p/c_V$, $\bar{\mu} = \mu/\mu^*$ and μ^* is a constant. The first factor $\bar{k}_0$ is calculated as

$$\bar{k}_0(\bar{T}) = \frac{\sqrt{\bar{T}}}{\sum_{i=0}^{4} \frac{I_i}{\bar{T}^i}}, \tag{2.66}$$

where I_i are constants. The second factor $\bar{k}_1$ is calculated as

$$\bar{k}_1(\bar{T}, \bar{\rho}) = \exp\left(\bar{\rho} \sum_{i=0}^{4} \left(\frac{1}{\bar{T}} - 1\right)^i \sum_{j=0}^{5} J_{ij}(\bar{\rho} - 1)^j\right), \tag{2.67}$$

where J_{ij} are constants. The last term, $\bar{k}_2$, is called the critical enhancement. Unlike the critical enhancement of the viscosity, this term plays a large role for the chosen temperatures and pressures and thus need to be accounted for properly. The term is described by

$$\bar{k}_2(\bar{T}, \bar{\rho}, \bar{c_p}, \lambda, \bar{\mu}) = \Lambda \frac{\bar{\rho}\bar{c_p}\bar{T}}{\bar{\mu}} Z(y), \tag{2.68}$$

where Λ is a constant. The function $Z(y)$ is described by

$$Z(y) = \begin{cases} \frac{2}{\pi y}\left(\left(1 - \frac{1}{\lambda}\right) + \frac{1}{\lambda} - 1 + \exp\left(\frac{-1}{\frac{1}{\lambda} + \frac{\lambda^2}{3\bar{\rho}^2}}\right)\right) & \text{if} \quad y > 1.2 \cdot 10^{-7} \\ 0 & \text{else} \end{cases} \tag{2.69}$$

The variable y on the other hand is calculated using

$$y = \bar{q}_D \xi(\bar{T}, \bar{\rho}), \tag{2.70}$$

where $\bar{q}_D$ is a constant added to make y a dimensionless number. The function ξ is defined as

$$\xi(\bar{T}, \bar{\rho}) = \xi_0 \left(\frac{\Delta\bar{\chi}(\bar{T}, \bar{\rho})}{\Gamma_0}\right)^{v/y}, \tag{2.71}$$

where Γ_0 and v are constants and

$$\Delta\bar{\chi}(\bar{T}, \bar{\rho}) = \bar{\rho}\left(\zeta(\bar{T}, \bar{\rho}) - \zeta(\bar{T}_R, \bar{\rho})\frac{\bar{T}_R}{\bar{T}}\right), \tag{2.72}$$

where $\bar{T}_R$ is a constant reference temperature and ζ is defined as

$$\zeta(\bar{T}, \bar{\rho}) = \left(\frac{\partial\bar{\rho}}{\partial\bar{p}}\right)_{\bar{T}} = \kappa_T \bar{\rho} p^*. \tag{2.73}$$

where p^* is a constant used to normalize the pressure. With equations (2.41) and (2.57), the density of water is obtained using the temperature and the pressure. The temperature and pressure is also used to calculate the isothermal compressibility through equations (2.44) and (2.60). However, to calculate ζ, κ_T needs to be calculated using the temperature and density as our starting point. With the equations described, this would require iteration on pressure until it matches the density. Instead, the industrial approximation is used to calculate $\zeta(\bar{T}_R, \bar{\rho})$. It is stated as

$$\zeta(\bar{T}_R, \bar{\rho}) = \frac{1}{\sum_{i=0}^{5} K_{ij} \bar{\rho}^i}, \tag{2.74}$$

where K_{ij} are constants. The index j is chosen as

$$\begin{cases} j = 0 & \text{if} \quad \bar{\rho} \leq 0.310559006 \\ j = 1 & \text{if} \quad 0.310559006 < \bar{\rho} \leq 0.776397516 \\ j = 2 & \text{if} \quad 0.776397516 < \bar{\rho} \leq 1.242236025 \\ j = 3 & \text{if} \quad 1.242236025 < \bar{\rho} \leq 1.863354037 \\ j = 4 & \text{if} \quad 1.863354037 < \bar{\rho}. \end{cases} \tag{2.75}$$

In the area of interest, the error in the estimation of thermal conductivity is between 1.5% and 6%. It increases as temperature increases.

2.4.4 Saturation line

The boundary between liquid water and steam is called the saturation line. In order to pass this line, latent heat needs to be added or removed from the fluid. With either temperature or pressure known, the other one can be calculated [16]. The constants n_i defined in Appendix A are used for this. If the saturation temperature T_s is known, the equation

$$\tau = \frac{T_s}{T^*} + \frac{n_9}{(T_s/T^*) - n_{10}}, \tag{2.76}$$

holds. Here, $T^* = 1\,\mathrm{K}$. The saturation pressure p_s is then

$$p_s = p^* \left(\frac{2\vartheta_3}{-\vartheta_2 + (\vartheta_2^2 - 4\vartheta_1\vartheta_3)^{1/2}} \right)^4, \tag{2.77}$$

where $p^* = 1\,\mathrm{MPa}$ and

$$\vartheta_1 = \tau^2 + n_1\tau + n_2 \tag{2.78}$$

$$\vartheta_2 = n_3\tau^2 + n_4\tau + n_5 \tag{2.79}$$

$$\vartheta_3 = n_6\tau^2 + n_7\tau + n_8. \tag{2.80}$$

If instead the saturation pressure is known, the equation

$$\pi = (p_s/p^*)^{1/4}, \tag{2.81}$$

holds. The saturation temperature is then

$$T_s = T^* \left(\frac{n_{10} + \beta_1 - ((n_{10} + \beta_1)^2 - 4(n_9 + n_{10}\beta_1))^{1/2}}{2} \right), \tag{2.82}$$

where

$$\beta_1 = \frac{2\beta_4}{-\beta_3 - (\beta_3^2 - 4\beta_2\beta_4)^{1/2}} \tag{2.83}$$

$$\beta_2 = \pi^2 + n_3\pi + n_6 \tag{2.84}$$

$$\beta_3 = n_1\pi^2 + n_4\pi + n_7 \tag{2.85}$$

$$\beta_4 = n_2\pi^2 + n_5\pi + n_8. \tag{2.86}$$

The latent heat needed for phase change is the difference between the specific enthalpies of the fluid at that temperature and pressure when it is a liquid and a gas. These are calculated as described in Sections 2.4.1 and 2.4.2, respectively.

2.5 Emissions

One of the main benefits proposed of the WET cycle is the reduction of emissions that impact the climate. Two emission types will be investigated; carbon dioxide and nitrogen oxides.

2.5.1 Carbon dioxide

Carbon dioxide (CO_2) is a potent greenhouse gas. It is produced in combustion of hydrocarbon based fuels, such as conventional jet fuel. The amount of CO_2 produced is directly proportional to the fuel usage. One way to reduce CO_2-emissions in the aviation industry is to make the propulsion systems more efficient. More efficient propulsion means less fuel usage, which means less CO_2-produced. This requires continuous research to increase the technology level of the propulsion systems. Another option is to switch fuel source, either to something that does not contain carbon such as liquid hydrogen, or to something that does not use combustion at all such as fuel cells or batteries. Liquid hydrogen comes with its own problems, such as a more complex process of handling cryogenic liquids as well as a very large volume requirement for the tanks. Batteries are also too heavy to be practical for long-range flight.

2.5.2 Nitrogen oxides

Nitrogen oxides (NO_x) are a group of gases that are relevant for air pollution. They are generated in all combustion with air due to the high abundance of nitrogen and oxygen in air, and the high temperatures involved in combustion. NO_x-emissions

are one of the main emissions from aircraft responsible for climate warming and tropospheric ozone [2]. The amount of NO_x-gas produced is calculated as a fraction of the amount of fuel used using the emissions index EI_{NOx} [4], through

$$\dot{m}_{NOx} = \dot{m}_{fuel} \cdot EI_{NOx} \quad [\text{g/s}]. \tag{2.87}$$

For humid combustion, the emission index is calculated as

$$EI_{NOx} = 32 \cdot \exp\left(\frac{T_{cc,in} - 826}{194}\right) \cdot \left(\frac{p_{cc,in}}{2.965 \cdot 10^6}\right)^{0.4} \cdot TF \cdot R_{STM} \quad [\text{g/kg}], \tag{2.88}$$

where $T_{cc,in}$ and $p_{cc,in}$ are the temperature and pressure of the air as it enters the combustion chamber, TF is the technology factor and R_{STM} is the steam correction factor. The technology factor is taken as $TF = 0.72$ for state-of-the-art engines. The steam correction factor is obtained as

$$R_{STM} = \exp\left(\frac{-2.465WAR^2 - 0.915WAR}{WAR^2 + 0.0516}\right), \tag{2.89}$$

where WAR is the water-to-air ratio of the reaction mixture as it enters the combustion chamber.

3
Methods

The project is divided into two part. The first part concerns the development of models for the WET cycle and a full system model of a WET cycle turbofan engine. The second part is comprised of the evaluation of the WET cycle using the previously developed model.

3.1 Component and system modelling

The model of the reference cycle, as well as all of the components that it consists of, were already available in GESTPAN at the start of the project. GESTPAN is a scientific tool developed for performance evaluation of aero engines [10]. It is based on defining and connecting modules that in themselves represent a single conceptual component of the engine. The modules interact with each other through input and output variables. It is important to note that during design each component in GESTPAN is intended to be set up as a quadratic system of equations. This means that, for each iteration variable that is solved in a given component, there is a corresponding residual that belongs to the same component. This also means that each component can be solved in order, without the need to relay information backwards and iterate. However, it is possible to include global iteration variables, where the iteration variable belongs to one component while the residual belongs to another.

3.1.1 Modifications to established components

Since GESTPAN was developed for regular aero engines, the main variables that represent the gas flow are temperature, pressure, mass flow and the fuel-to-air ratio (FAR). In order to take into account the injected water, the water-to-air ratio (WAR) was added, which is the ratio of the injected mass flow of water to the mass flow of air. Note that the WAR does not include water that is produced by combustion. It was also assumed that air that enters the engine is dry, such that the only components that needed to be updated with the WAR are the burner and the components after it. With this modification, the amount of air, fuel and water in the flow were calculated as

$$\dot{m}_{air} = \frac{\dot{m}}{1 + FAR + WAR} \tag{3.1}$$

$$\dot{m}_{fuel} = \frac{FA\dot{R} \cdot m}{1 + FAR + WAR} \tag{3.2}$$

$$\dot{m}_{water} = \frac{WA\dot{R} \cdot m}{1 + FAR + WAR}. \tag{3.3}$$

All tables used to obtain thermodynamic properties of the flow were also updated to include WAR.

3.1.2 Heat Recovery Steam Generator

The equations for the different sections of the HRSG are similar. The properties of the water as it enters the HRSG were assumed to be known. The properties of the exhaust gas as it exits the HRSG was also assumed to be known. On a system level these properties are not known, but becomes iteration variables. However, for the component calculations, they were regarded as known. For the economizer, the exit temperature of the water is the saturation temperature at that water pressure, which was obtained from Section 2.4.4. The thermodynamic properties and the transport properties of the exhaust gas and the water were found as described in Section 2.4. The heat transfer was calculated by a simple energy balance between the hot side and cold side, using (2.9). The heat transfer coefficient was estimated using the approach described in Section 2.3.2. For simplicity, the entry variables were used when estimating the heat transfer coefficient. With this, the wetted area that has been used for the economizer section was calculated with (2.12).

The calculations for the evaporator followed the same structure as for the economizer. However, due to the phase change in the fluid, the heat transfer for the water side was instead calculated using (2.10). Since the evaporator handles both liquid and gas in the same channel, it is difficult to estimate the thermodynamic properties. Instead, the properties were calculated individually for the liquid and for the gas. This gave two heat transfer coefficients and two pressure losses. In order to not underestimate the pressure losses, the maximum pressure loss was chosen. For the heat transfer coefficients, a combined coefficient was calculated using [11]

$$\begin{aligned} \frac{h(x)}{h_{liquid}} = \Bigg(& (1-x)^{0.01} \left((1-x)^{1.5} + 1.9 x^{0.6} \left(\frac{\rho_{liquid}}{\rho_{gas}} \right)^{0.35} \right)^{-2.2} + \\ & + x^{0.01} \left(\frac{h_{gas}}{h_{liquid}} \left(1 + 8(1-x)^{0.7} \left(\frac{\rho_{liquid}}{\rho_{gas}} \right)^{0.67} \right) \right)^{-2} \Bigg)^{-0.5}, \end{aligned} \tag{3.4}$$

where x is the fraction of all the fluid that is liquid. Numerical integration along the evaporator is required to know the liquid fraction at each point. For simplicity, it was assumed that there is an even split between liquid and gas in the evaporator. Equation (3.4) has been obtained for boiling of liquids in vertical tubes. However,

in this investigation, a large variety of heat exchangers are examined. The equation was thus used outside of what it has been designed for.

The calculations for the superheater were similar to the ones for the economizer and evaporator. At the design point, the exit temperature of the water is given as a design parameter. With the sensible heat transfer of both of the channels, from (2.9), as well as the heat transfer calculated using the LMTD-method, from (2.12), the wetted area of the water channel was obtained.

In off-design the total wetted area is fixed. Together with the wetted areas used to economize and evaporate the water, the wetted area that remains was calculated as

$$A_{superheater} = A - A_{economizer} - A_{evaporator}. \tag{3.5}$$

In this case, none of the exit temperatures are known. On the other hand, the area that the superheater uses is known. The exit temperatures of the superheater were iterated on with residuals given as the difference between the heat given off and taken up by the exhaust gas and the water respectively, using (2.9), as well as the heat calculated by the LMTD-method, using (2.12).

It was assumed that the ratio of wetted area of a section to the total wetted area for the HRSG is the same as the ratio of the length of the section to the total length of the HRSG. Thus, the length of section i were calculated as

$$L_i = L \cdot \frac{A_i}{A}. \tag{3.6}$$

With the lengths known, the pressure drops over the sections were calculated as described in Section 2.3.2.

3.1.3 Condenser

For the condenser, the exhaust gas inlet conditions and the cooling gas outlet conditions were assumed to be known. Since it is a counter flow heat exchanger that consists of multiple sections, it is important to know the inlet conditions of one fluid and the outlet conditions of the other fluid in order to be able to calculate each section consecutively. For the economizer section, the temperature of the exhaust gas as it exits is the temperature at the saturation point and was obtained through the methods in Section 2.4. Sensible heat transfer between the two channels then gave the entry temperature of the coolant into the economizer, and through the method described in Section 2.3.2 together with the LMTD-method, the wetted area needed to achieve this was calculated.

For the condenser section the approach differed depending on whether the design point or off-design was considered. At the design point, there is a design requirement on the amount of water that should be condensed. The WRF gave the ideal mass flow rate of water given the design flow rate. The total amount of water in the exhaust flow entering the condensing section is both the water produced by combustion and the water injected into the combustion chamber. The ideal amount of water still left in the exhaust flow was then calculated as the difference between the total amount of water flowing into the condensing section and the

ideal condensed water. This ideal amount of water left in the exhaust flow dictates the partial pressure of the water at the exit, which in turn is related to the saturation temperature at that partial pressure. This relation is described in Section 2.4.4. Using an enthalpy balance before and after the condensing section, the heat transfer and in turn the temperature of the cooling air as it enters the condenser was calculated. The LMTD-method then gave the wetted area used for condensing.

For off-design, the workflow of the condensing section was the opposite. The area used for condensing was calculated by

$$A_{condensing} = A - A_{economizing}. \tag{3.7}$$

Iteration on the exit temperature of the exhaust gas was then done, with the residual error taken as the difference between the heat transfer necessary to condense the water and the heat transfer calculated with the LMTD-method. The entry temperature of the coolant as well as the amount of water condensed was then calculated using the exit temperature.

3.1.4 System considerations

The system model of the WET cycle, from the burner onwards, can be viewed in Figure 3.1. If the model was to be constructed only for the design point, the WAR in the burner, which is specified for the design point, would be known and all components could be calculated one after the other. However, in off-design, it is not possible to know how much water will be condensed, which makes it impossible to know how much water is injected into the combustion chamber. The amount of water that is condensed is itself a function of how much water was injected, further complicating the issue. Thus, it was necessary to iterate on the amount of injected water until the injected flow of water and the flow of condensed water were equal. This residual was placed in the pump, as this is the last component to be computed.

Further iteration variables were needed in order to solve the system due to the assumptions made when constructing the burner, HRSG and condenser modules. To start with, the temperature of the water as it is injected into the combustion chamber needs to be known by the burner module, but can't be known before the HRSG has been calculated. Thus, it became an iteration variable that was solved by an internal residual in the HRSG, matching the iteration variable with the calculated output temperature. The inlet temperature of the water was assumed to be known for the calculations of the HRSG, but due to the order of operations it is not known before the pump has been calculated. To solve that, an iteration variable for the HRSG was introduced, with a corresponding residual in the pump.

The iteration variables mentioned are global iteration variables, where the variable and the residual end up in different components and can not be solved for unless all components are run multiple times. However, due to the definitions there was also a few local iteration variables introduced. Firstly, the HRSG equations assumes that the exhaust outlet conditions are known. Assuming a low pressure loss, this is true except for the temperature which was iterated on. Secondly, the condenser equations assumes that all of the cooling outlet conditions are known.

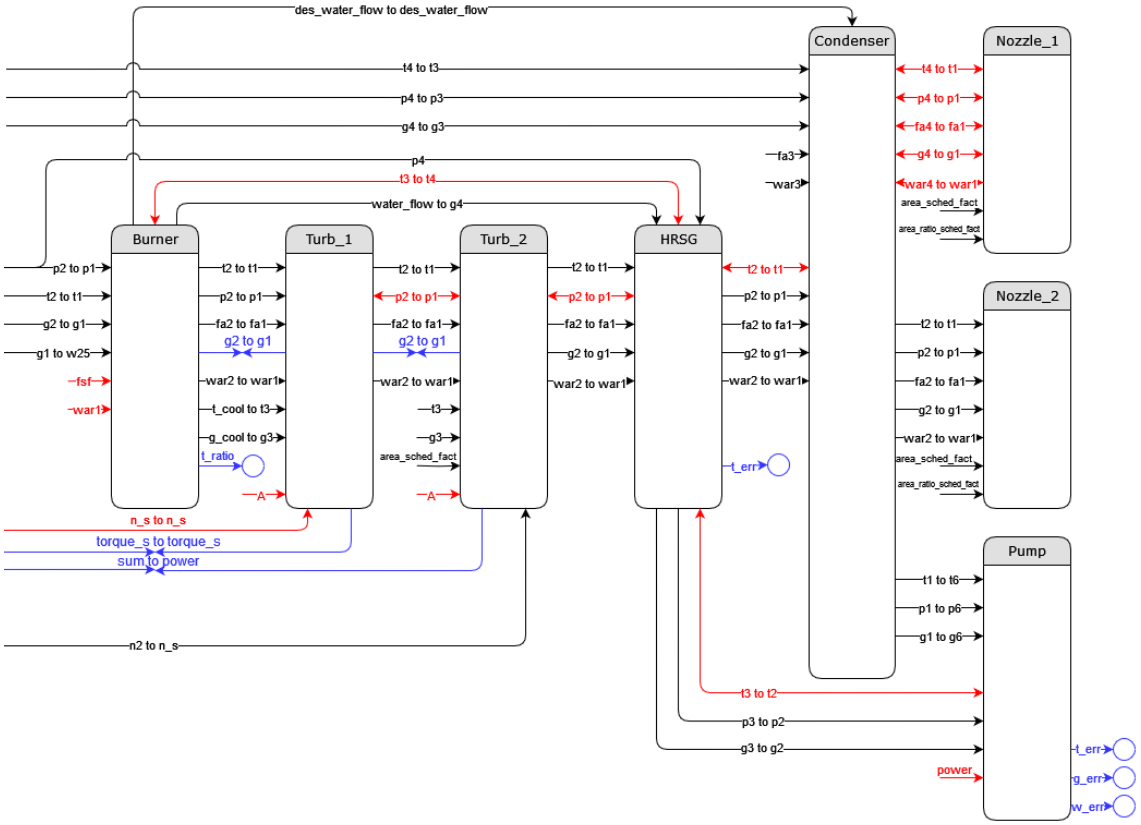

Figure 3.1: The modules that the WET-engine model consists of and the flow of data between the modules. Red connections indicate an iteration variable and blue connections indicate a residual. For simplicity, only modules and connections from the burner onwards are shown, and the overall-module was removed. For a full connection diagram, see Appendix B.

All of these variables need to be iterated in, and were solved in the condenser alone since the inlet variables were used to match against.

One way to reduce the number of iteration variables would be to switch the order in which the sections of the HRSG are calculated. This would mean that the variables that are assumed to be known are the inlet conditions of the exhaust and the outlet conditions of the water. This is true except for the mass flow and temperature of the water. However, iterating on the outlet temperature of the water can give temperatures below freezing if the initial value is set too far away from the correct value. This causes the solver to do unexpected things, and does not lead to a good solution. Instead it is more robust to iterate on the inlet conditions of the water, since the inlet temperature is generally in a small band of temperatures.

3.2 System performance evaluation

In order to evaluate the performance of the WET cycle, some design parameters were chosen as parameters of interest. These were varied in order to optimize the engine with respect to specific fuel consumption (SFC). Optimization was carried

out at the design point of the engine, which was Top-of-Climb (TOC). The chosen variables were the turbine inlet temperature (T_4), the bypass ratio (BPR), the water-to-air ratio (WAR) at the design point, and the temperature of the injected water (T_{inj}). Furthermore, the generalized geometric parameters (GGP) of the two heat exchangers were varied to minimize their weight given the performance requirements. The parameters of interest and the researched bounds are provided in Table 3.1.

Cycle	
Parameter	**Range**
T_4 (K)	1200-2000
BPR	10-30
WAR (%)	0-30
T_{inj} (K)	500-1000

HRSG GGP	
Parameter	**Range**
α_r	0.1-2.0
σ_r	0.1-1.0
χ	0.1-0.4

Condenser GGP	
Parameter	**Range**
α_r	0.1-2.0
σ_r	0.1-1.0
χ	0.1-0.4

Table 3.1: Variables of interest during the optimization of the WET cycle turbofan and their respective bounds.

In the reference engine, the high pressure turbine (HPT) is cooled using a bypass stream from the high pressure compressor (HPC). The second turbine is, however, uncooled. The exhaust gas temperature entering the second turbine can thus not be higher than what the turbine blades allow. To avoid this, the inlet temperature of the second turbine in the cycle was limited to the inlet temperature of the second turbine in the reference engine, which sets a limit on T_4. Varying the optimization parameters also affects the mass flow of air used for a given thrust. A larger area is needed to accommodate a larger amount of air flow, which requires more space underneath the aircraft wing. The reference engine is a large engine, and it was thus assumed that increasing the size of the engine is not feasible, so the mass flow of air in the WET cycle engine was limited to the mass flow of air in the reference cycle. It was assumed that, with a BPR and T_4 determined for a fixed WAR, an optimal T_{inj} exists with respect to SFC.

For the new components, some parameters had to be estimated. All estimated parameters can be seen in Table 3.2. For the heat exchangers in both the HRSG and the condenser, the characteristic dimension ($\frac{l_f}{\sqrt{t_f}}$), the wall thickness (t_w) and the free-flow distance (ℓ) were taken as estimated by Miltén for a turbofan intercooler.

Additionally, the heat transfer coefficients of the heat exhangers estimated using the approach in Section 2.3.2 were increased by 10% due to the estimation being based on historical data. The calculated masses of the heat exchangers were also increased by 10% to account for piping, bulkheads and other structural elements. The frontal area of the HRSG was estimated from the available area of the core, and the frontal area of the condenser was estimated to the area of the bypass channel. The Water Recovery Factor (WRF) of the condenser is difficult to determine, but was taken to be 90%. The efficiency of the pump was taken to be 90%.

HRSG	
Parameter	**Value**
$\frac{l_f}{\sqrt{t_f}}$	0.45 $m^{1/2}$
t_w	0.5 mm
ℓ	1 cm
A_{fr}	0.5 m^2
h	+10%
m_s	+10%

Condenser	
Parameter	**Value**
$\frac{l_f}{\sqrt{t_f}}$	0.45 $m^{1/2}$
t_w	0.5 mm
ℓ	1 cm
A_{fr}	8.6 m^2
h	+10%
m_s	+10%
WRF	90%

Pump	
Parameter	**Value**
η	90%

Table 3.2: Constants used for the WET cycle specific components.

4
Results

In this chapter, the results for the WET cycle engine are presented and compared against the reference engine. The results show the effect of the chosen design variables on cycle performance, the effect of heat exchanger GGPs on the component weights, and the resulting performance after optimization. The reference cycle was not analyzed as it was assumed to be at a local optimum.

4.1 Initial cycle observations

Simulations were run in which the bypass ratio and turbine inlet temperature were varied while the water-to-air ratio and water injection temperature were held constant for the WET cycle. How the SFC varies for the reference cycle and for the WET cycle is seen in Figure 4.1. The point with lowest SFC lies at the intersection between the size limit line and the heat limit line. The size limit line is where the airflow exactly matches the airflow of the reference engine, given a fixed thrust. Being above the size limit line means that more air flow is required, which would require a larger engine which is not feasible. The heat limit line represents where the turbine inlet temperature of the second turbine matches what is achieved in the reference engine. Increased turbine inlet temperature of the first turbine also increased the turbine inlet temperature of the second turbine. Since the second turbine is not cooled, the temperature needs to be below the temperature limit of the turbine blades, which creates a heat limit on the inlet temperature of the first turbine. The heat limit was constant with varying BPR and water injection temperature, but changed with WAR as the specific heat capacity of the core flow changed, which decreased the temperature drop over the first turbine. The power limit line is where the power available in the core flow for the turbines matches the power required to drive the compressors. It is not possible to have a higher BPR or a lower turbine inlet temperature than the power line, as the turbines would not be able to generate the necessary power to drive the compressors.

It is visible that a lower turbine inlet temperature and a higher BPR lead to a lower SFC. However, due to the power and size limits, it was preferable to increase the turbine inlet temperature to the heat limit. This allowed for the highest possible BPR, which in turn gave the lowest possible SFC. As WAR increased, the intersection between the size limit and the heat limit increased in BPR and decreased in turbine inlet temperature.

To determine a suitable water injection temperature, simulations were done for varying WAR in which the turbine inlet temperature was increased to the heat

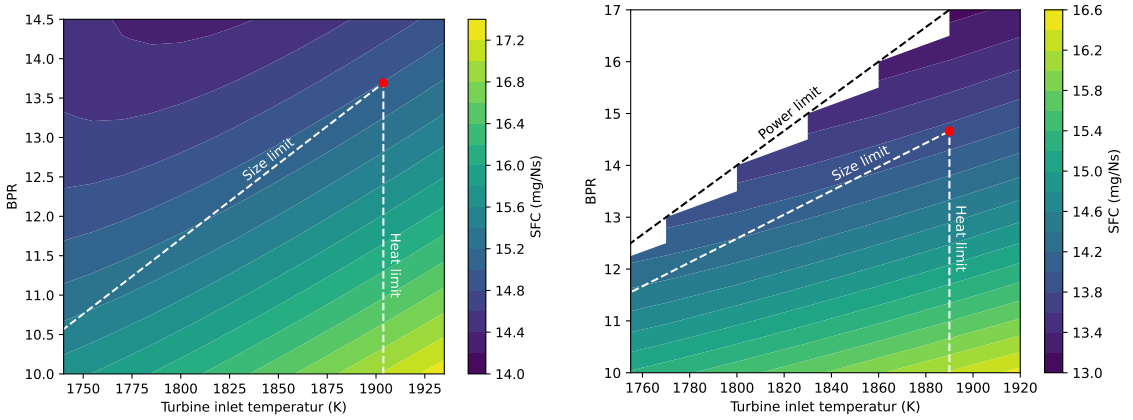

(a) Reference

(b) WAR = 0%

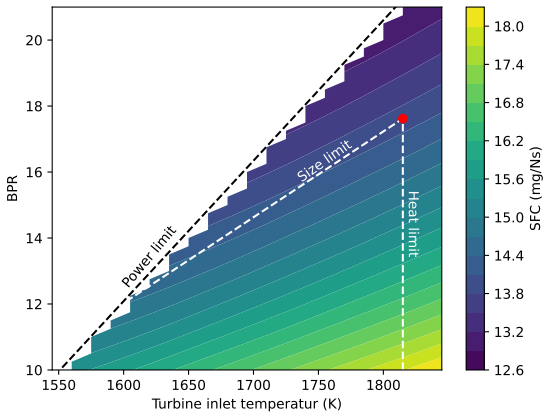

(c) WAR = 10%

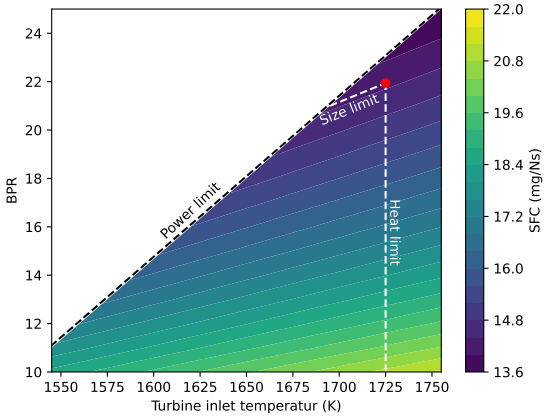

(d) WAR = 30%

Figure 4.1: SFC with varying turbine inlet temperature and bypass ratio for the reference cycle and for the WET cycle. The red dot represents the point with lowest SFC within the feasible zone. Simulations of the WET cycle were done for multiple WAR at the same water injection temperature (T_{inj} = 600 K).

limit and the bypass ratio was increased to the size limit. The resulting turbine inlet temperature, BPR and SFC for these simulations is seen in Figure 4.2. As T_{inj} increased, the BPR at the chosen design point decreased. The BPR differed more from the reference line at higher WAR. T_4 either increased or decreased for the reference line depending on the WAR. However, while BPR changed with as much as 4% in the investigated area, T_4 stayed within 0.05% from the reference. The effect of T_{inj} on SFC was similarly small, with the largest change for a single WAR in the investigated area being 0.35%. The T_{inj} that gave the lowest SFC varied with WAR, being higher at low WAR than at high WAR.

Choosing the simulation for each WAR with the lowest SFC, the data set shown in Figure 4.3 was obtained. T_{inj} followed an exponential curve. As WAR increased, the T_{inj} with lowest SFC decreased and approached 500 K, which is the boiling temperature of water at the pressure inside the HRSG.

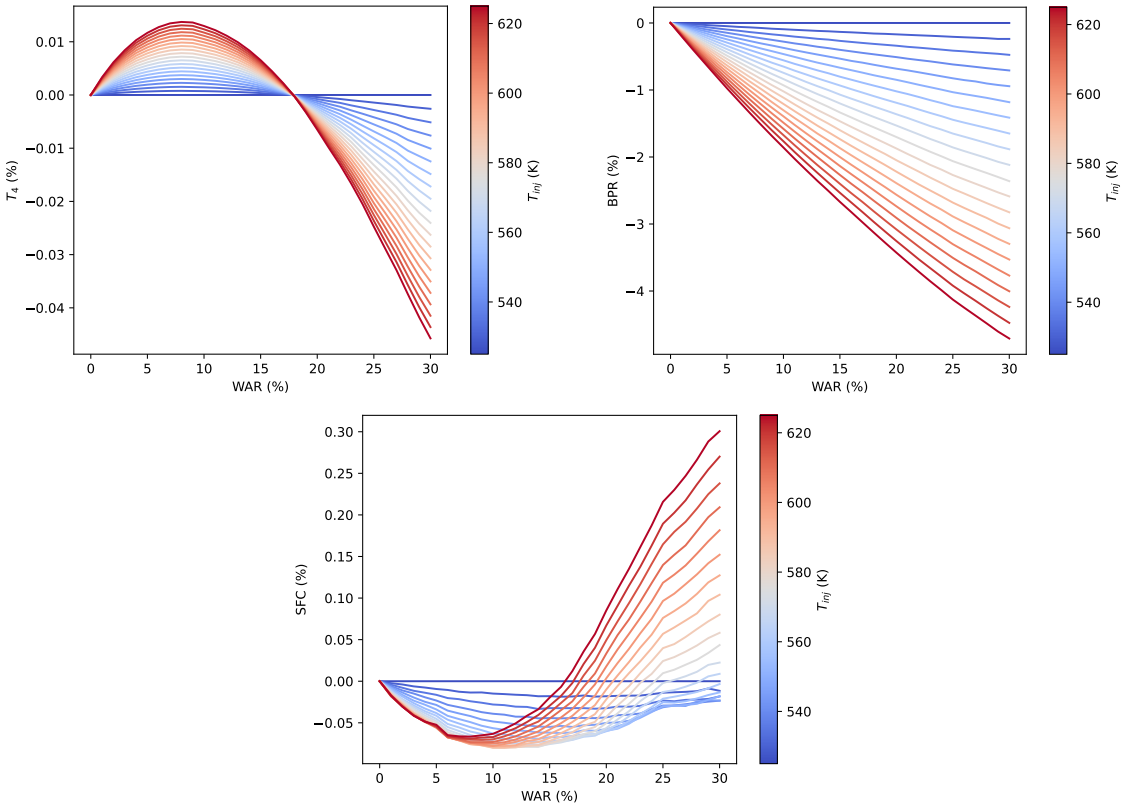

Figure 4.2: T_4, BPR and SFC for WAR from 0% to 30% and T_{inj} from 525 K to 625 K. Data is normalized against the results for the simulations carried out at $T_{inj} = 525$ K, and differences are presented in percent.

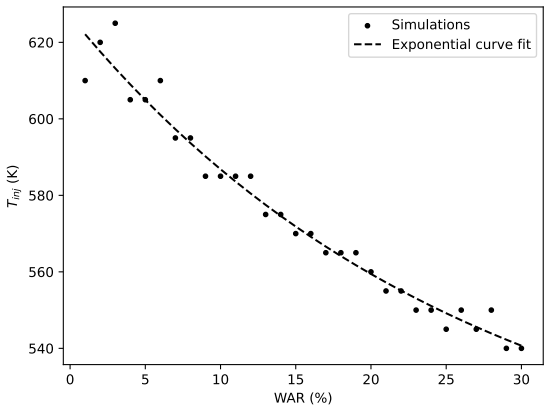

Figure 4.3: The simulation with the lowest SFC for each WAR, with an exponential curve fit of the data. The exponential curve follows the formula $T_{inj} = 500 + 127 \cdot e^{-3.79 \cdot \mathrm{WAR}}$, where WAR is given as a fraction.

4.2 Heat exchanger weight minimization

Parameter	HRSG	Condenser
α_r	1.37	0.73
σ_r	0.8	0.5
χ	0.1	0.1

Table 4.1: Optimal GGPs with respect to HX weight minimization for reference case.

In order to determine the best heat exchanger parameters for the HRSG and the condenser, a reference case was used where BPR and T_4 were the same as for the reference cycle, T_{inj} = 650 K and WAR = 10%. The GGP that resulted in the lowest weight for each of the heat exchangers are presented in Table 4.1. For the HRSG, a high α_r and a similarly high σ_r, with a low χ, gave the lowest weight. The behaviour of the condenser was different. Although a low χ was still preferred, a lower σ_r and a much lower α_r gave the lowest weight.

4.3 Optimized WET cycle

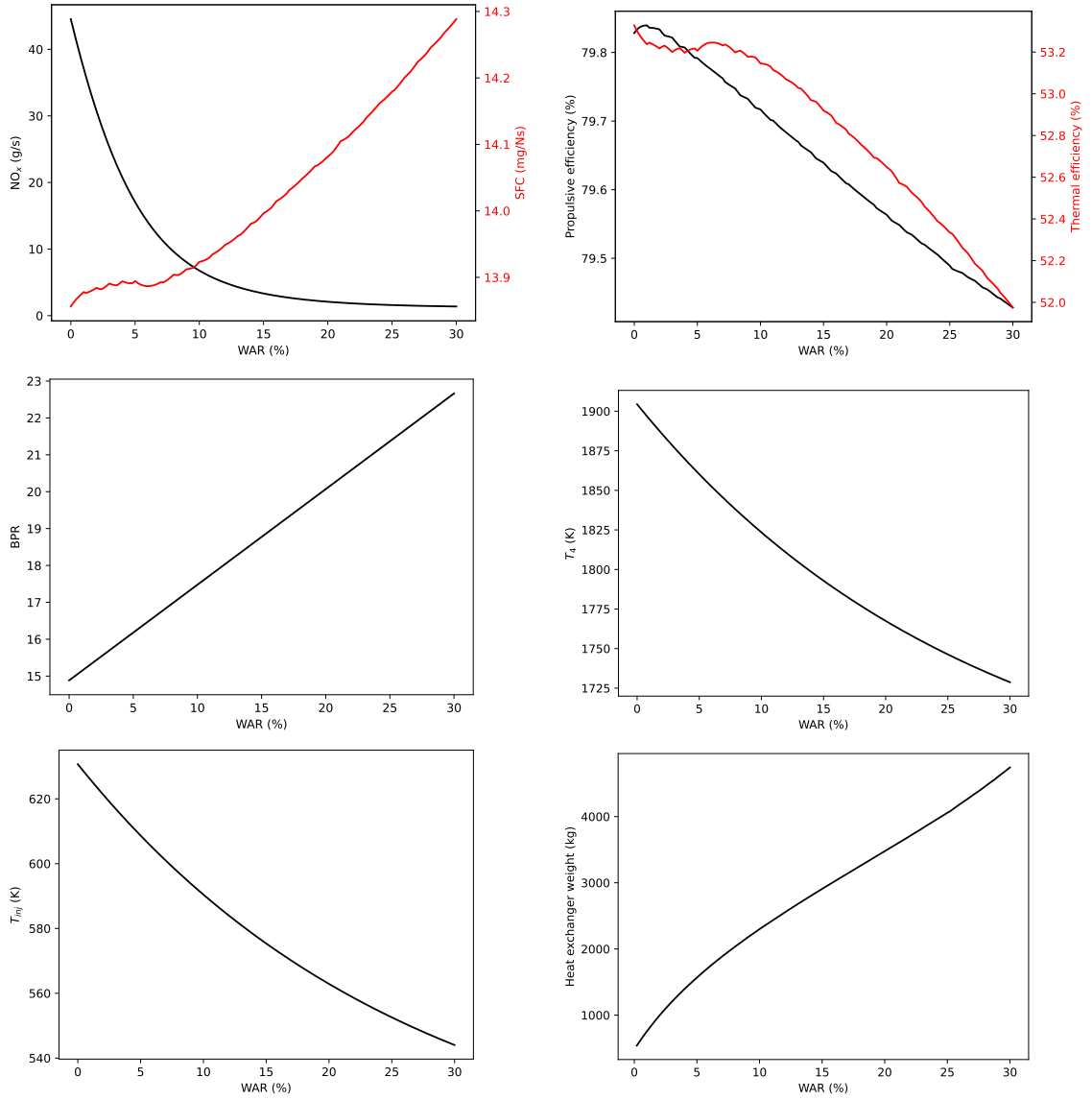

Figure 4.4: Design parameters (BPR, T_4 and T_{inj}), NO_x-emissions, SFC, propulsive efficiency η_p, thermal efficiency η_{th} and heat exchanger weights for the optimized engine configuration.

The results from Section 4.1 were used to find the optimal engine configuration for a given WAR, with respect to SFC. The results from Section 4.2 were used to determine the parameters to use for the components specific to the WET cycle. The results from this is presented in Figures 4.4 and 4.5. As is seen, the point with the lowest SFC occured when no water was added to the combustion. Throughout the investigated area, the SFC was lower than for the reference cycle. The NO_x-emissions had the opposite behaviour. The most NO_x was produced when no water was added, and the emissions continuously decreased as more water was added. Both the propulsive efficiency and the thermal efficiency decreased with as WAR

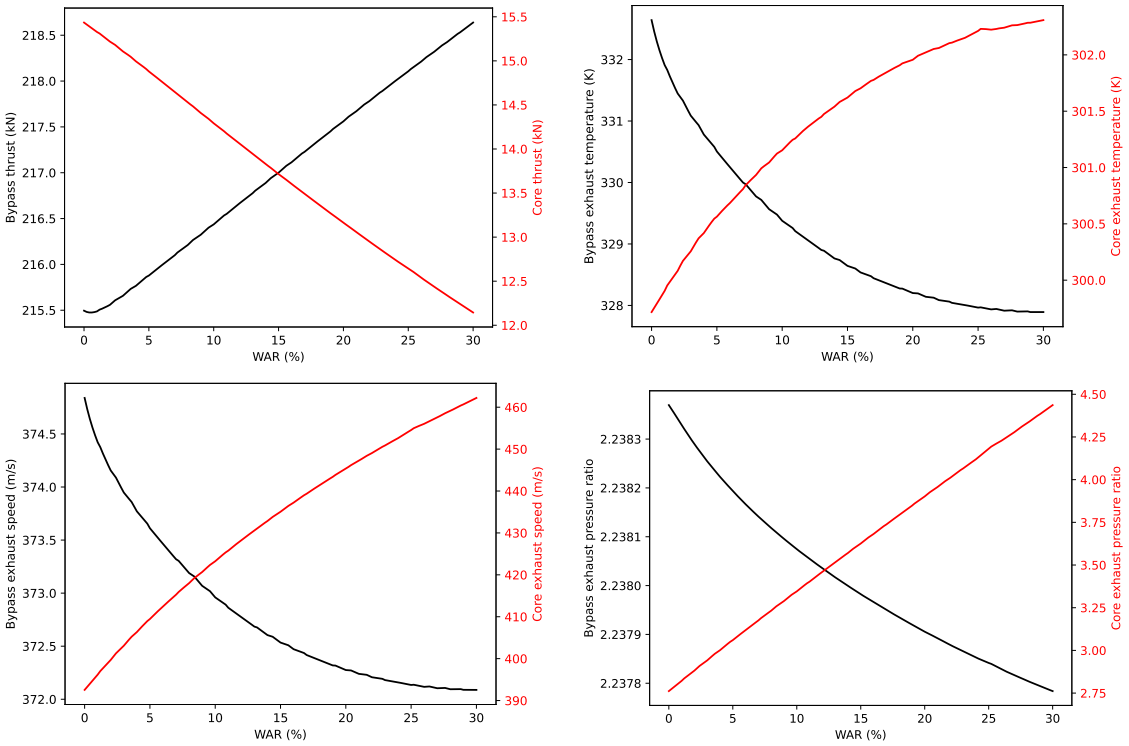

Figure 4.5: Comparison of thrust, exhaust temperature, exhaust speed and exhaust pressure ratio between the bypass flow and the core flow.

increased. However, the drop in thermal efficiency over the investigated zone was over three times larger than the drop in propulsive efficiency. As the water content increased, the BPR increased linearly, while the turbine inlet temperature and water injection temperature decreased exponentially. The weight of the heat exchangers continuously increased with the water content of the exhaust.

As WAR increased, more thrust was produced in the bypass nozzle and less thrust was produced in the core nozzle. For the bypass, both the temperature and the speed of the exhaust gas decreased, but for the core flow, the temperature and the speed of the exhaust increased. The pressure ratio between the flow and the atmosphere of the bypass nozzle decreased very slightly as WAR increased, however, the pressure ratio of the core flow nozzle increased significantly.

Further information is provided in Table 4.2. The three selected cycles are compared against the reference cycle. For the first case, there was a drop in SFC and a rise in BPR. There was also a significant decrease in core exhaust temperature, with a corresponding rise in bypass exhaust temperature. Similarly, the core exhaust speed showed a significant decrease while the bypass exhaust speed increased. The amount of NO_x-gases produced also decreased. For the other two cases, the SFC decreased compared to the reference engine but not as much as the former case. However, the BPR had a much higher increase, rising with more than 65% for the case when WAR=30%. The same trends with exhaust speed and exhaust temperature were still observed in these cases, although slightly smaller. The NO_x-production decreased by more than 85% for these cases. The fuel-to-air ratio also increased significantly, which was not observed when WAR=0%.

Parameter	**Reference**	**WAR=0%**	**WAR=10%**	**WAR=30%**
SFC (mg/Ns)	15.006	-7.7%	-7.2%	-4.8%
BPR	13.693	+8.7%	+27.6%	+65.5%
T_4 (K)	1903.8	-	-4.2%	-9.2%
Fuel flow (kg/s)	1.0703	-7.4%	-7.2%	-4.7%
Burner FAR (%)	3.0165	+0.1%	+16.7%	+53.4%
Bypass T (K)	292.54	+13.7%	+12.6%	+12.1%
Bypass v (m/s)	351.14	+6.8%	+6.2%	+6.0%
Bypass π	2.2385	-	-	-
Core T (K)	845.05	-64.5%	-64.4%	-64.2%
Core v (m/s)	709.03	-44.6%	-40.3%	-34.8%
Core π	3.2669	-15.5%	+2.4%	+35.8%
NO_x (g/s)	48.098	-7.4%	-85.9%	-97.1%
η_p	0.71607	+11.5%	+11.3%	+10.9%
η_{th}	0.54894	-2.9%	-3.2%	-5.3%

Table 4.2: Values of important parameters for WAR=0%, WAR=10% and WAR=30%, compared to the reference engine. Changes smaller than ±0.1% are displayed as -.

Information specific to the WET cycle for the three cases can be seen in Table 4.3. As WAR increased, the heat duty of the HRSG increased as well as the weight and volume of the component. However, the relationship is different for the condenser. As WAR increased, the heat duty decreased slightly, while the weight and volume increased.

Parameter	WAR=0%	WAR=10%	WAR=30%
HRSG heat transfer (MW)	-	8.3621	18.474
HRSG volume (m^3)	-	1.1543	4.6850
HRSG weight (kg)	-	342.71	1390.9
HRSG ΔT_{lm} (K)	319.24	291.09	209.00
Condenser heat transfer (MW)	23.670	21.928	21.286
Condenser volume (m^3)	1.1543	6.5929	11.288
Condenser weight (kg)	630.70	1957.4	3351.3
Condenser ΔT_{lm} (K)	112.50	85.604	39.702
Pump power (kW)	-	8.5242	19.780
Water inlet temperature (K)	(630.7)	590.44	544.02

Table 4.3: Values of important WET cycle specific parameters for WAR=0%, WAR=10% and WAR=30%. Some parameters are not applicable when no water is injected.

5
Discussion

The results show some similarities with previous studies, but also exhibit behaviour that has not previously been reported.

5.1 Cycle parameter characteristics

For a conventional turbofan engine, SFC decreases as BPR increases. For the WET cycle, a higher BPR was achieved than for the reference engine. Partly, this was because the injected water was a large part of the core flow, so less air from the inlet was needed in order to carry the energy from the combustion chamber and disperse it along the turbines. The core air flow is only needed for combustion and for thrust from the core nozzle, but thrust is also produced in the bypass nozzle. However, water also has a higher specific heat capacity, which means that less total flow is required to carry the same amount of heat energy. The BPR has to conform to the size limit of the engine. A too high BPR leads to a mass flow that is larger than the mass flow of the reference engine, given a low turbine inlet temperature. A larger mass flow of air requires a larger diameter engine. In order to allow for the highest possible BPR and follow the size limit, the turbine inlet temperature was increased until the inlet temperature of the second turbine reached the heat limit of the turbine blades. The higher specific heat capacity of the flow when water is added results in a lower temperature drop across the turbines. Due to this, the allowed turbine inlet temperature decreased as the water content increased. Although a high BPR is seen as preferable, it was not possible to achieve a BPR of 34.5 which was stated in the concept article [4]. Relaxation of the heat limit constraint allowed for higher turbine inlet temperature and a similar BPR to the concept article. However, this requires other solutions for cooling the low pressure turbine. Relaxation of the size limit constraint alone did not yield a high enough BPR, as the power limit became the new limiting factor.

In the results, the water injection temperature was chosen based on minimization of SFC, together with an exponential fit of the available simulation data. However, SFC had a very weak correlation to the water injection temperature, while the injection temperature increased the weight of the HRSG. In order to minimize additional weight, it is preferable to remove super-heating at the design point. As shown in Figure 4.2, this gave at most a penalty in SFC of 0.1%. In the concept article, a steam turbine was placed between the HRSG and the water injector [4]. The water pump then increased the pressure when the water was liquid. The steam is then expanded through the steam turbine, which lowers the temperature and

pressure of the steam. This made it possible to utilize heat in the steam to produce work for the low pressure shaft. It only required extra work from the water pump, which is cheap in terms of power as the water is liquid. It is possible that a higher temperature of the steam as it exits the HRSG is more favourable in such a configuration.

5.2 Fuel consumption and emissions

The presented data shows a large drop in SFC when the engine type was switched from the reference cycle to the WET cycle, while no water was injected. As more water was injected, the SFC increased. As CO_2-emissions are proportional to SFC they followed the same trend. This indicates that the largest benefit in terms of SFC and CO_2-emissions came from the condenser heat exchanger, as it transported energy from the core flow to the bypass flow. The addition of water in turn had a negative impact on SFC. Compared to previous research [5], this result is unexpected and indicates that cycle performance can be further improved. The efficiency is further analysed in Section 5.4.

Furthermore, the SFC specified does not take into account the installation effects of the WET cycle specific components. As the HRSG and condenser can contribute significantly to the weight of the engine, this will increase the weight of the final aircraft and in turn its fuel consumption. The weight of the heat exchangers increased the more water they needed to be able to handle, which would further incentivize selecting a low WAR. The weight of the HRSG was in line with previous research [12]. The condenser was lighter than previous research [12]. No study of how the additional weight of the heat exchangers impact the fuel consumption was made.

The NO_x-emissions also showed a decrease simply from the introduction of the heat exchangers. However, this reduction can be attributed to the lowered fuel consumption due to the drop in SFC. As more water was added a much larger decrease in NO_x-emissions was achieved, down to less than 3% of the emissions of the reference cycle inside the investigated zone. As SFC increased and NO_x-emissions decreased with as water injection increased, it was preferable to find a point where both factors were taken into account. At WAR=10%, the SFC was reduced by 7.2% form the reference cycle, which is still close to the minimum SFC achieved at WAR=0%. However, the drop in NO_x-emissions was 85.9%, which is significantly more than when WAR=0%.

5.3 Heat exchangers

The weight of the heat exchangers depended heavily on the GGP chosen when they were designed. It is also clear that the GGP that minimized weight for a specific mission differed between the two components. This shows that the method used to calculate the heat exchangers successfully captured the different fluids and processes involved in the two heat exchangers, and changed the optimal design accordingly. An α_r that was further away from unity in the HRSG than in the condenser suggests

more uneven distribution of the wetted area between the two channels in the HRSG than in the condenser. This is reasonable as there are is one liquid and one gas present in the HRSG, and heat transfer from liquid to solid is easier than heat transfer from gas to solid. On the other hand, the σ_r was lower in the condenser than in the HRSG. This means that the distribution of free-flow area between the two channels was more uneven in the condenser than in the HRSG. This is also reasonable, as the condenser handles an exhaust flow which is much smaller than the bypass flow, given the high BPR.

The heat duty of the HRSG increased as more water was added to the combustion. This led to a corresponding increase in weight. Another factor that contributed to this was the decrease in logarithmic mean temperature difference (ΔT_{lm}). As more water was added to the exhaust, the specific heat capacity of the flow increased, which resulted in a lower temperature drop for a given heat duty. A lower ΔT_{lm} means that a larger area is needed for the same amount of heat transfer, provided that the heat transfer coefficient is unaffected. The condenser also increased in weight as the amount of injected/condensed water increased. However, unlike for the HRSG, the heat duty decreased slightly. When more water was added, the temperature out from the low pressure turbine increased as the heat capacity of the flow increased. In the HRSG on the other hand, more water was provided for cooling, so the net result was that the temperature of the exhaust flow into the condenser decreased. Although more water needed to condense, and the exit temperature needed to decrease in order for all the water to condense, the decrease in inlet temperature resulted in a decrease in the heat transfer. The increase in weight can instead be explained by the ΔT_{lm}, which decreased as the inlet temperature decreased, which in turn required a larger heat exchanger to keep up with the heat duty.

5.4 Thrust generation and efficiency

The propulsive efficiency of a turbofan cycle is a measure of how well the kinetic energy is used to generate thrust, and depends on the flow velocity and the nozzle exit pressures [20]. For the WET cycle with no water injection, it is evident that the heat exchangers transported heat from the core flow to the bypass flow, when compared to the reference cycle. This decreased the temperature and the speed of sound of the core flow, and since the nozzle is choked it means that the flow speed decreased as well. This increased the propulsive efficiency of the core flow, as it is more efficient to produce thrust at low flow velocity than at high. Although, it also decreased the core thrust. For the bypass, the added energy increased temperature and flow velocity, but not by as much as for the core as there was more fluid to absorb the energy. This partly decreased the efficiency of the bypass, but more importantly it increased the thrust. Thus, more thrust was produced in the more efficient bypass nozzle, and less thrust was produced in the less efficient core nozzle, while at the same time the core nozzle became more efficient. In total, it meant a higher propulsive efficiency. As WAR increased, the benefit of increased propulsive efficiency decreased slightly. This can be explained by the increase in pressure ratio in the core nozzle. As water injection changes the fluid properties, the pressure of the exhaust was higher as it exited the turbines than it was when no water was

added. More water further increased the pressure after the turbines. The HRSG and the condenser that comes after the turbines mainly lowered the temperature without affecting the pressure, so the pressure of the exhaust as it entered the nozzle increased, and the pressure ratio with the atmospheric pressure increased.

The largest drop in efficiency came from the thermal efficiency. When the reference cycle was switched for the WET cycle, the thermal efficiency dropped, and when the amount of injected water increased, it dropped further. The WET cycle, as investigated, had a fuel consumption that was 4.7-7.4% less than for the reference cycle. This means that less energy was added to the cycle, which is good for thermal efficiency. However, looking at the isentropic exhaust speeds of the nozzles, it is seen that the core speed went down while the bypass speed went up when the reference cycle was switched for the WET cycle. In the end, this meant that the kinetic energy in the exhaust stream was less in the WET cycle than in the reference cycle. As WAR increased, the fuel consumption went up which made the thermal efficiency go down further. One of the proposed benefits of the HRSG was that it transfers heat back to the combustion chamber which keeps it within the cycle [4], [5]. If the steam is hotter, less fuel needs to be used to reach the same turbine inlet temperature which increases the thermal efficiency. This effect could however not be replicated.

5.5 Limitations

The investigated cycle differed from the proposed concept on a few points. Due to the time constraint, the investigated cycle did not have a steam turbine. The role of a steam turbine is to utilize the recovered heat to drive the low power shaft [4]. A high water outlet temperature from the HRSG becomes favourable with a steam turbine, as that means more power for the steam turbine to use. As no steam turbine was implemented, nothing like this was seen. Another difference from the concept is the relatively high overall pressure ratio (OPR). It has been observed that the WET cycle allows for lower OPR [4], [5], [12], however, since OPR was not investigated the original high OPR of the reference cycle was used. Initial studies showed no indication of a preference for low OPR, and the parameter was thus not selected for further investigation. However, a lower OPR might show promise when combined with other parameters that were also not investigated, such as the amount of cooling flow or the pressure ratios of the individual compressors. Other differences that could affect the results are that the investigated cycle had an intermediate pressure compressor, while the concept does not specify one [4]. The investigated cycle also used all of the bypass air for cooling in the condenser, while the concept used a portion of the bypass air.

It is difficult to model the condenser as it involves multi-phase flow, phase transitions and recovery of water droplets from the exhaust gas flow. There are a number of improvements that can be made to the condenser model. As of now, no work has been done to identify what factors impact the water recovery factor (WRF). The WRF is however a very important parameter for the condenser as it determines the size. If the WRF is too low, the condenser also becomes unfeasible as there is not enough water in the flow to condense all of the injected water. In

the current study, it was also assumed that the condenser always condenses the same amount of water that was injected. In reality, the amount of injected water would need to be controlled to keep up with the available water, and so losses will occur. At the beginning of the work, it was assumed that the condenser would be significantly longer than the distance between the core and the nacelle and be tilted forward. Correspondingly, the condenser was modelled as a counter-flow heat exchanger. However, the length of the condenser was slightly shorter than the core-to-nacelle distance. The exhaust gas is thus flowing perpendicular to the bypass flow, and the condenser would be better represented as a cross-flow heat exchanger.

Both the HRSG and condenser had problems with the estimation of pressure losses. In the current model, the pressure losses were on the order of a few Pascals, which is smaller than what would reasonably be expected. Any effects arising from the pressure losses from the addition of heat exchangers were thus not visible in the results. Consequently, the Meredith effect could not be assessed. Furthermore, the heat exchanger model was based on geometry-specific parameters such as the undisturbed flow length (ℓ) and the characteristic dimension ($\frac{l_f}{\sqrt{t_f}}$). These are difficult to estimate for a finished heat exchanger design, and is even more difficult to estimate for a general case. They also displayed a great impact on the performance of the heat exchangers.

The methodology of the optimization brought with it certain disadvantages. SFC was the variable that was being optimized in all steps except for the last, in which NO_x-emissions was also considered. However, SFC considers the cycle efficiency of the engine and does not take into account installation effects of the heat exchangers. The introduction of heavy heat exchangers will require more thrust from the engines, which will burn more fuel. Moreover, the current optimization was carried out at the design point, which in this case was Top-of-Climb due to the specification of the reference engine. For most of the flight time of the aircraft, it will be flying in cruise condition, so most emission will happen there. It is also important to make sure that the engine works well at sea level and during take-off. These factors should be considered in future works.

6
Conclusion

The aim of this project has been to model the components that constitute a WET cycle engine in the modelling tool GESTPAN and to use these components to model the whole cycle. The full cycle model was to be used to evaluate the benefits of having steam injection and water recovery in a turbofan engine. After this, future areas of research were to be identified.

In order to perform the work, a simplified cycle was used where the steam turbine was removed. The full system model was based on a geared, two-spool, high bypass ratio turbofan design developed for the year 2035, which also was used as a reference cycle. The heat exchangers were modeled using a new method developed for a general heat exchanger and that is based on non-dimensional geometric parameters. Both the HRSG and the condenser were assumed to be counter-flow heat exchangers. To model the heat exchangers proved challenging as some key geometric parameters are hard to estimate. The condenser was especially difficult to model as no detailed studies of the behaviour of the water recovery process was found.

The results showed that, with well chosen parameters, the SFC and CO_2-emissions were reduced by 7.2% and NO_x-emissions were reduced by 85.9%, with a total added mass of 2300 kg for heat exchangers. This result was achieved with a low combustion chamber WAR of 10%. The largest benefit in terms of SFC came from the addition of the condenser, which increased the propulsive efficiency of the cycle by moving energy from the core flow to the bypass flow. On the other hand, the largest benefit in terms of NO_x-emissions came from the addition of water in the combustion chamber as the increased amounts of water lowered the combustion temperature and prevented the formation of NO_x-gases.

The cycle was limited by the size of the engine and by the temperature at the LPT inlet. At the most optimal point found using the chosen variables, SFC increased as the amount of water injected increased. It is thought that this trend is due to the limit on turbine inlet temperature, which in turn limited the BPR. The results for thrust generation also showed that the pressure ratio in the core channel increased as the amount of water injected increased. It is proposed that cooling of the LPT should be investigated in order to allow for a higher turbine inlet temperature. It is also proposed to investigate the choice of OPR, as this has been an important parameter for the WET cycle in previous research.

This work confirms the benefits proposed by the concept article, and it shows some limitations that need to be considered when designing a WET cycle engine. In order to take full advantage of the steam injection, more parameters need to be considered.

Bibliography

[1] J. E. Green, "Air Travel – Greener by Design Mitigating the environmental impact of aviation: Opportunities and priorities," *The Aeronautical Journal*, vol. 109, no. 1099, pp. 361–416, 2005. DOI: 10.1017/S0001924000000841.

[2] U. Schumann, "The impact of nitrogen oxides emissions from aircraft upon the atmosphere at flight altitudes—results from the aeronox project," *Atmospheric Environment*, vol. 31, no. 12, pp. 1723–1733, 1997, ISSN: 1352-2310. DOI: 10.1016/S1352-2310(96)00326-3.

[3] M. Gauss, I. S. A. Isaksen, D. S. Lee, and O. A. Søvde, "Impact of aircraft NO_x emissions on the atmosphere - tradeoffs to reduce the impact," *Atmospheric Chemistry and Physics*, vol. 6, no. 6, pp. 1529–1548, 2006. DOI: 10.5194/acp-6-1529-2006.

[4] S. Kaiser, O. Schmitz, P. Ziegler, and H. Klingels, "The Water-Enhanced Turbofan as Enabler for Climate-Neutral Aviation," *Applied Sciences*, vol. 12, no. 23, 2022. DOI: 10.3390/app122312431.

[5] O. Schmitz, H. Klingels, and P. Kufner, "Aero Engine Concepts Beyond 2030: Part 1—The Steam Injecting and Recovering Aero Engine," *Journal of Engineering for Gas Turbines and Power*, vol. 143, 2021. DOI: 10.1115/1.4048985.

[6] R. Pouzolz, O. Schmitz, and H. Klingels, "Evaluation of the Climate Impact Reduction Potential of the Water-Enhanced Turbofan (WET) Concept," *Aerospace*, vol. 8, no. 3, 2021. DOI: 10.3390/aerospace8030059.

[7] L. Sun, Q. Zheng, Y. Li, M. Luo, and R. K. Bhargava, "Numerical Simulation of a Complete Gas Turbine Engine With Wet Compression," *Journal of Engineering for Gas Turbines and Power*, vol. 135, 2013. DOI: 10.1115/1.4007366.

[8] V. G. Gkoutzamanis, M. K. Psaropoulos, and A. I. Kalfas, "AIRCRAFT ENGINE PERFORMANCE AUGMENTED BY WET COMPRESSION," in *Turbomachinery Technical Conference & Exposition*, ASME, 2023.

[9] M. Jonsson and J. Yan, "Humidified gas turbines—a review of proposed and implemented cycles," *Energy*, vol. 30, pp. 1013–1078, 2005. DOI: 10.1016/j.energy.2004.08.005.

[10] T. Grönstedt, C. Xisto, X. Zhao, *et al.*, "Multidisciplinary assessment of a year 2035 turbofan propulsion system," in *33rd Congress of the International Council of the Aeronautical Sciences*, ICAS, vol. 7, 2022, pp. 4981–4990.

[11] VDI-Gesellschaft Verfahrenstechnik und Chemieingenieurwesen, *VDI Heat Atlas*, 2nd ed. Springer-Verlag Berlin Heidelberg, 2010, ISBN: 978-3-540-77876-9. DOI: 10.1007/978-3-540-77877-6.

[12] M. Sakic and M. Nitulescu, *Steam generation and exhaust water recovery for the Water Enhanced Turbofan (WET)*, 2021.

[13] H. Qiao, "Correction of Log Mean Temperature Difference Method and Effectiveness-NTU Relations for Two-phase Heat Transfer with Pressure Drop and Temperature Glide," in *International Refrigeration and Air Conditioning Conference*, 2018.

[14] I. J. Karassik, J. P. Messina, P. Cooper, and C. C. Heald, *Pump Handbook*, 3rd ed. McGRAW-HILL, 2001, ISBN: 0-07-034032-3.

[15] P. Miltén, I. Johnsson, A. Lundbladh, and C. Xisto, "GENERALIZED METHOD FOR THE CONCEPTUAL DESIGN OF COMPACT HEAT EXCHANGERS," in *Turbomachinery Technical Conference & Exposition*, ASME, 2024.

[16] *Revised Release on the IAPWS Industrial Formulation 1997 for the Thermodynamic Properties of Water and Steam*, The International Association for the Properties of Water and Steam, 2007.

[17] *Revised Advisory Note No. 3 - Thermodynamic Derivatives from IAPWS Formulations*, The International Association for the Properties of Water and Steam, 2018.

[18] *Release on the IAPWS Formulation 2008 for the Viscosity of Ordinary Water Substance*, The International Association for the Properties of Water and Steam, 2008.

[19] *Release on the IAPWS Formulation 2011 for the Thermal Conductivity of Ordinary Water Substance*, The International Association for the Properties of Water and Steam, 2011.

[20] T. Grönstedt, C. Xisto, X. Zhao, and M. Thoma, "An introduction to the wonderful world of aerospace propulsion," 2023.

A

Constants for water properties

A.1 Liquid water

$p^* = 16530000$ Pa, $T^* = 1386$ K, $R = 461.526$ J/kg K

i	I_i	J_i	n_i
1	0	-2	0.14632971213167
2	0	-1	-0.84548187169114
3	0	0	-0.37563603672040e1
4	0	1	0.33855169168385e1
5	0	2	-0.95791963387872
6	0	3	0.15772038513228
7	0	4	-0.16616417199501e-1
8	0	5	0.81214629983568e-3
9	1	-9	0.28319080123804e-3
10	1	-7	-0.60706301565874e-3
11	1	-1	-0.18990068218419e-1
12	1	0	-0.32529748770505e-1
13	1	1	-0.21841717175414e-1
14	1	3	-0.52838357969930e-4
15	2	-3	-0.47184321073267e-3
16	2	0	-0.30001780793026e-3
17	2	1	0.47661393906987e-4
18	2	3	-0.44141845330846e-5
19	2	17	-0.72694996297594e-15
20	3	-4	-0.31679644845054e-4
21	3	0	-0.28270797985312e-5
22	3	6	-0.85205128120103e-9
23	4	-5	-0.22425281908000e-5
24	4	-2	-0.65171222895601e-6
25	4	10	-0.14341729937924e-12
26	5	-8	-0.40516996860117e-6
27	8	-11	-0.12734301741641e-8
28	8	-6	-0.17424871230634e-9
29	21	-29	-0.68762131295531e-18
30	23	-31	0.14478307828521e-19
31	29	-38	0.26335781662795e-22

32	30	-39	-0.11947622640071e-22
33	31	-40	0.18228094581404e-23
34	32	-41	-0.93537087292458e-25

Table A.1: Liquid water constants.

A.2 Steam

$p^* = 1000000$ Pa, $T^* = 540$ K, $R = 461.526$ J/kg K

i	J_i°	n_i°
1	0	-0.96927686500217e1
2	1	0.10086655968018e2
3	-5	-0.56087911283020e-2
4	-4	0.71452738081455e-1
5	-3	-0.40710498223928
6	-2	0.14240819171444e1
7	-1	-0.43839511319450e1
8	2	-0.28408632460772
9	3	0.21268463753307e-1

Table A.2: Steam J_i° and n_i° constants.

i	I_i	J_i	n_i
1	1	0	-0.17731742473213e-2
2	1	1	-0.17834862292358e-1
3	1	2	-0.45996013696365e-1
4	1	3	-0.57581259083432e-1
5	1	6	-0.50325278727930e-1
6	2	1	-0.33032641670203e-4
7	2	2	-0.18948987516315e-3
8	2	4	-0.39392777243355e-2
9	2	7	-0.43797295650573e-1
10	2	36	-0.26674547914087e-4
11	3	0	0.20481737692309e-7
12	3	1	0.43870667284435e-6
13	3	3	-0.32277677238570e-4
14	3	6	-0.15033924542148e-2
15	3	35	-0.40668253562649e-1
16	4	1	-0.78847309559367e-9
17	4	2	0.12790717852285e-7
18	4	3	0.48225372718507e-6
19	5	7	0.22922076337661e-5
20	6	3	-0.16714766451061e-10
21	6	16	-0.21171472321355e-2

22	6	35	-0.23895741934104e2
23	7	0	-0.59059564324270e-17
24	7	11	-0.12621808899101e-5
25	7	25	-0.38946842435739e-1
26	8	8	0.11256211360459e-10
27	8	36	-0.82311340897998e1
28	9	13	0.19809712802088e-7
29	10	4	0.10406965210174e-18
30	10	10	-0.10234747095929e-12
31	10	14	-0.10018179379511e-8
32	16	29	-0.80882908646985e-10
33	16	50	0.10693031879409
34	18	57	-0.33662250574171
35	20	20	0.89185845355421e-24
36	20	35	0.30629316876232e-12
37	20	48	-0.42002467698208e-5
38	21	21	-0.59056029685639e-25
39	22	53	0.37826947613457e-5
40	23	39	-0.12768608934681e-14
41	24	26	0.73087610595061e-28
42	24	40	0.55414715350778e-16
43	24	58	-0.94369707241210e-6

Table A.3: Steam I_i, J_i and n_i constants.

A.3 Viscosity

$T^* = 647.096$ K, $\rho^* = 322$ kg/m^3, $\mu^* = 1.0$e-6 Pa s

i	F_i
0	1.67752
1	2.20462
2	0.6366564
3	-0.241605

Table A.4: Viscosity F_i constants.

i	j	G_{ij}
0	0	5.20094e-1
1	0	8.50895e-2
2	0	-1.08374
3	0	-2.89555e-1
0	1	2.22531e-1
1	1	9.99115e-1
2	1	1.88797

3	1	1.26613
5	1	1.20573e-1
0	2	-2.81378e-1
1	2	-9.06851e-1
2	2	-7.72479e-1
3	2	-4.89837e-1
4	2	-2.57040e-1
0	3	1.61913e-1
1	3	2.57399e-1
0	4	-3.25372e-2
3	4	6.98452e-2
4	5	8.72102e-3
3	6	-4.35673e-3
5	6	-5.93264e-4

Table A.5: Viscosity G_{ij} constants. Omitted values are identically equal to zero.

A.4 Thermal conductivity

$p^* = 22064000$ Pa, $T^* = 647.096$ K, $\rho^* = 322$ kg/m^3, $k^* = 1.0$e-3 W/m K, $\mu^* = 1.0$e-6 Pa s, $R = 461.51805$ J/kg K, $\Lambda = 177.8514$, $\overline{q_D}1 = 0.4$e-9 m, $v = 0.630$, $\gamma = 1.239$, $\xi_0 = 0.13$e-9 m, $\Gamma_0 = 0.06$, $\bar{T}_R = 1.5$

i	I_i
0	2.443221e-3
1	1.323095e-2
2	6.770357e-3
3	-3.454586e-3
4	4.096266e-4

Table A.6: Thermal conductivity I_i constants.

i	j	J_{ij}
0	0	1.60397357
0	1	-0.646013523
0	2	0.111443906
0	3	0.102997357
0	4	-0.0504123634
0	5	0.00609859258
1	0	2.33771842
1	1	-2.78843778
1	2	1.53616167
1	3	-0.463045512
1	4	0.0832827019
1	5	-0.00719201245

2	0	2.19650529
2	1	-4.54580785
2	2	3.55777244
2	3	-1.40944978
2	4	0.275418278
2	5	-0.0205938816
3	0	-1.21051378
3	1	1.60812989
3	2	-0.621178141
3	3	0.0716373224
3	4	0.0
3	5	0.0
4	0	-2.7203370
4	1	4.57586331
4	2	-3.18369245
4	3	1.1168348
4	4	-0.19268305
4	5	0.012913842

Table A.7: Thermal conductivity J_{ij} constants.

i	j	K_{ij}
0	0	6.53786807199516
0	1	6.52717759281799
0	2	5.35500529896124
0	3	1.55225959906681
0	4	1.11999926419994
1	0	-5.61149954923348
1	1	-6.30816983387575
1	2	-3.96415689925446
1	3	0.464621290821181
1	4	0.595748562571649
2	0	3.39624167361325
2	1	8.08379285492595
2	2	8.91990208918795
2	3	8.93237374861479
2	4	9.88952565078920
3	0	-2.27492629730878
3	1	-9.82240510197603
3	2	-12.03387295057900
3	3	-11.03219600611260
3	4	-10.32550511470400
4	0	10.26318546627090
4	1	12.13584137913950
4	2	9.19494865194302
4	3	6.16780999933360

4	4	4.66861294457414
5	0	1.97815050331519
5	1	-5.54349664571295
5	2	-2.16866274479712
5	3	-0.965458722086812
5	4	-0.503243546373828

Table A.8: Thermal conductivity K_{ij} constants.

A.5 Saturation line

$p^* = 1000000$ Pa

i	n_i
1	0.11670521452767e4
2	-0.72421316703206e6
3	-0.17073846940092e2
4	0.12020824702470e5
5	-0.32325550322333e7
6	0.14915108613530e2
7	-0.48232657361591e4
8	0.40511340542057e6
9	-0.23855557567849
10	0.65017534844798e3

Table A.9: Saturation line constants.

B

System model

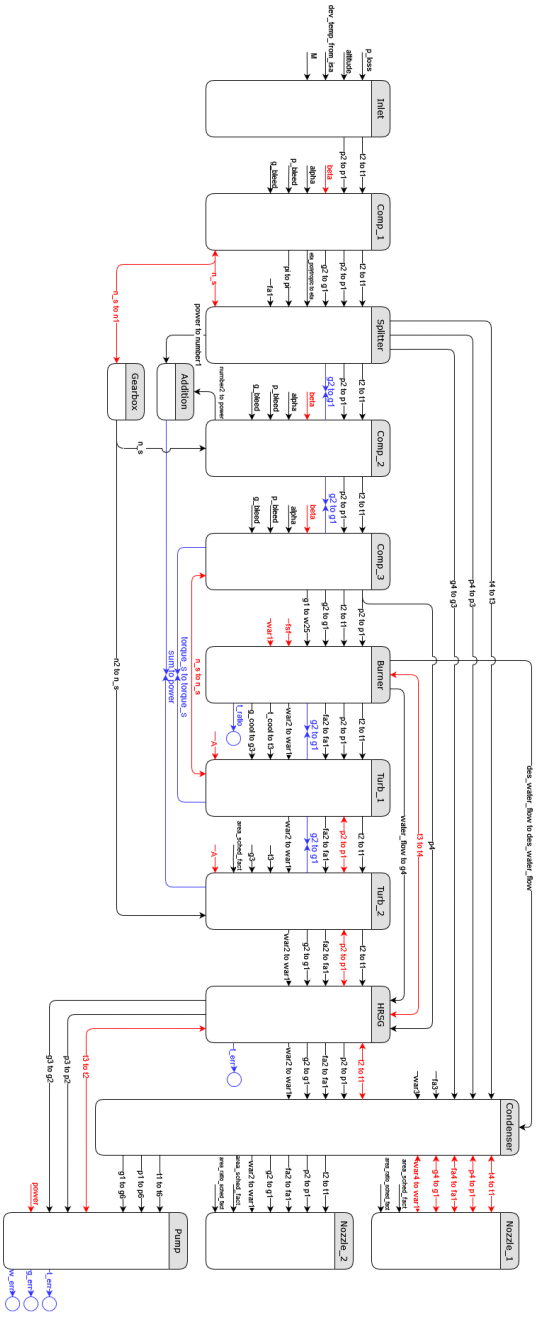

Figure B.1: Full system model.

DEPARTMENT OF MECHANICS AND MARITIME SCIENCES
CHALMERS UNIVERSITY OF TECHNOLOGY
Gothenburg, Sweden
www.chalmers.se

CHALMERS
UNIVERSITY OF TECHNOLOGY